Comparison of Static and Dynamic Pile Load Tests at Thi Vai International Port in Viet Nam

Le Phan Ta, *Ph.D student, Graduate School of Kanazawa University, Japan (HCMC University of Architecture, Viet Nam); email: phantale2002@yahoo.com*
Tatsunori Matsumoto, *Professor, Graduate School of Kanazawa University, Japan; email: matsumot@t.kanazawa-u.ac.jp*
Ha Nguyen Hoang, *Engineer, South Vietnam Bridge Road Building Technology Institute, Viet Nam; email: halasxd55@gmail.com*

ABSTRACT: *A berth structure, 600 m long and 60 m wide, for handing of loaded containers was completed in early 2013 as one of the facilities of Thi Vai International Port located on the bank of the Cai Mep river in Viet Nam. The berth is a quay structure supported by 885 driven spun concrete piles and 156 driven steel pipe piles. Four test piles, named TSC1, TSC2, TSP1 and TSP2, with different pile lengths and diameters were driven at the project site in 2011 prior to construction of working piles. Static load tests (SLTs) were conducted for the test piles to determine the design pile capacity. Dynamic load tests (DLTs) were also carried out for the TSC1 and TSP1 in order to obtain information for selecting the pile driving system used for the working piles and to examine the applicability of wave matching analysis (WMA) to derive the static load-displacement curves. A wave matching analysis program developed by the authors was employed in the WMAs. Good agreement between the derived and measured static responses was obtained for the TSC1 and TSP1. The identified soil parameters obtained from the final WMA of the TSC1 and TSP1 were used to predict the static responses of the TSC2 and TSP2. The predicted load-displacement curves were reasonable matches to the measured ones, indicating that the identified soil parameters of the test piles could be used for prediction of the static responses of other constructed piles. Moreover, pile driving termination criterion in this site was examined through the test piling.*

KEYWORDS: static load test, dynamic load test, steel pipe pile, spun concrete pile, wave matching analysis, pile foundation quality control, berth area

SITE LOCATION: IJGCH-database.kmz (requires Google Earth)

INTRODUCTION

Thi Vai International Port located on the bank of the Cai Mep river in Viet Nam (Fig. 1) is under construction, with the scheduled start of operation at the end of 2013. A berth structure, 600 m long and 60 m wide, has been completed in the project as shown in Fig. 2. The berth is a quay structure supported by 885 driven spun concrete piles (SC pile hereafter) and 156 driven steel pipe piles (SP pile hereafter). Test piling was conducted at the project site in 2011 to obtain design parameters, to select appropriate driving system, and to seek driving controls and quality assessment methods for constructed piles.

Four test piles were driven prior to construction of working piles. Two of them were spun concrete piles designated as TSC1 and TSC2, and the other two piles were open-ended steel pipe piles designated as TSP1 and TSP2. The TSC1 and TSC2 had outer diameters of 0.7 m and 0.8 m, wall thicknesses of 100 mm and 110 mm, and lengths of 54 m and 48.7 m, respectively. The TSP1 and TSP2 had outer diameters of 1.0 m and 0.9 m, respectively, a wall thickness of 12 mm, and lengths of 60 m and 49.9 m, respectively. All the test piles were driven using a diesel hammer having a ram mass of 10 tons. Dynamic load tests (DLTs) were carried out at the end of initial driving (EOD) and re-striking tests were conducted after curing periods of 7 days for the TSC1 and 34 days for the TSP1. Static load tests (SLTs) were carried out 10 days later for the TSC1 and 14 days later for the TSP1. SLT was also carried out for the TSC2 and TSP2 after the corresponding curing time of 17 days and 27 days from the completion of the driving work.

Submitted: 19 April 2013; Published: 26 August 2013
Reference: Phan, T.L., Matsumoto, T., and Nguyen, H.H. (2013). *Comparison of Static and Dynamic Pile Load Tests at Thi Vai International port in Viet Nam.* International Journal of Geoengineering Case histories, http://casehistories.geoengineer.org, Vol.3, Issue 1, p.36-66. doi: 10.4417/IJGCH-03-01-04

This paper first describes the test piling in detail including objectives, site conditions, preliminary pile design and results of the SLTs. Then, wave matching analysis (WMA) of the DLTs at initial driving and re-striking are conducted using a numerical approach developed by the authors, in order to derive the corresponding static load-displacement relations and soil resistance distributions. The derived load-displacement relations clearly showed so-called "set-up" phenomena. The derived load-displacement relations of the TSC1 and TSP1 were good estimates for the results of the SLTs. Static load-displacement relations of the TSC2 and TSP2 were predicted using the soil parameters identified from the WMA of the TSC1 and TSP1, respectively. The predicted results were comparable to the measured results, indicating that DLT with WMA is a good alternative to SLT.

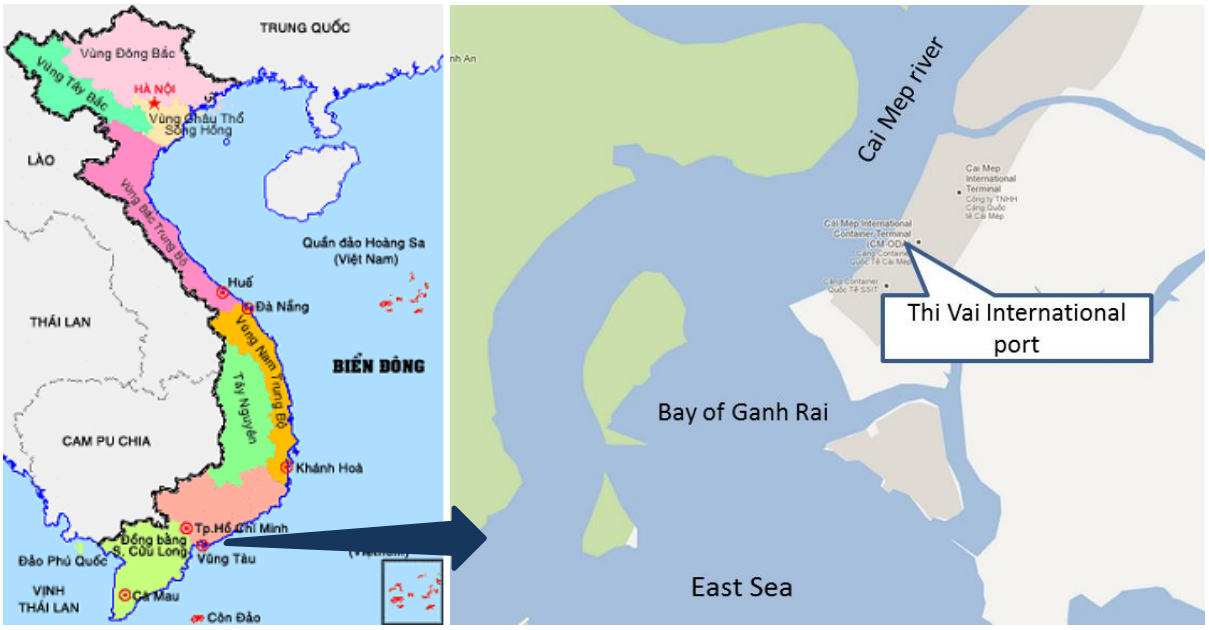

Figure 1. Location of the site (with Vietnam on the left).

Figure 2. Photo of the berth area prior to use.

SITE AND TEST DESCRIPTION

Site conditions

Locations of the boreholes, working piles and test piles, and geological sections at the four test piles

A total of the 30 borehole investigations were conducted in this area (Fig. 3) to obtain the profiles of the soil layers and SPT *N*-values. Typically, very soft clay exists from the seabed to depths of 6 m to 20 m. Below this top layer, a clayey sand of about 25 m thickness ranging from a loose state at the top to medium dense state at the bottom is present. It is underlain by hard silt clay that could be regarded as a bearing stratum.

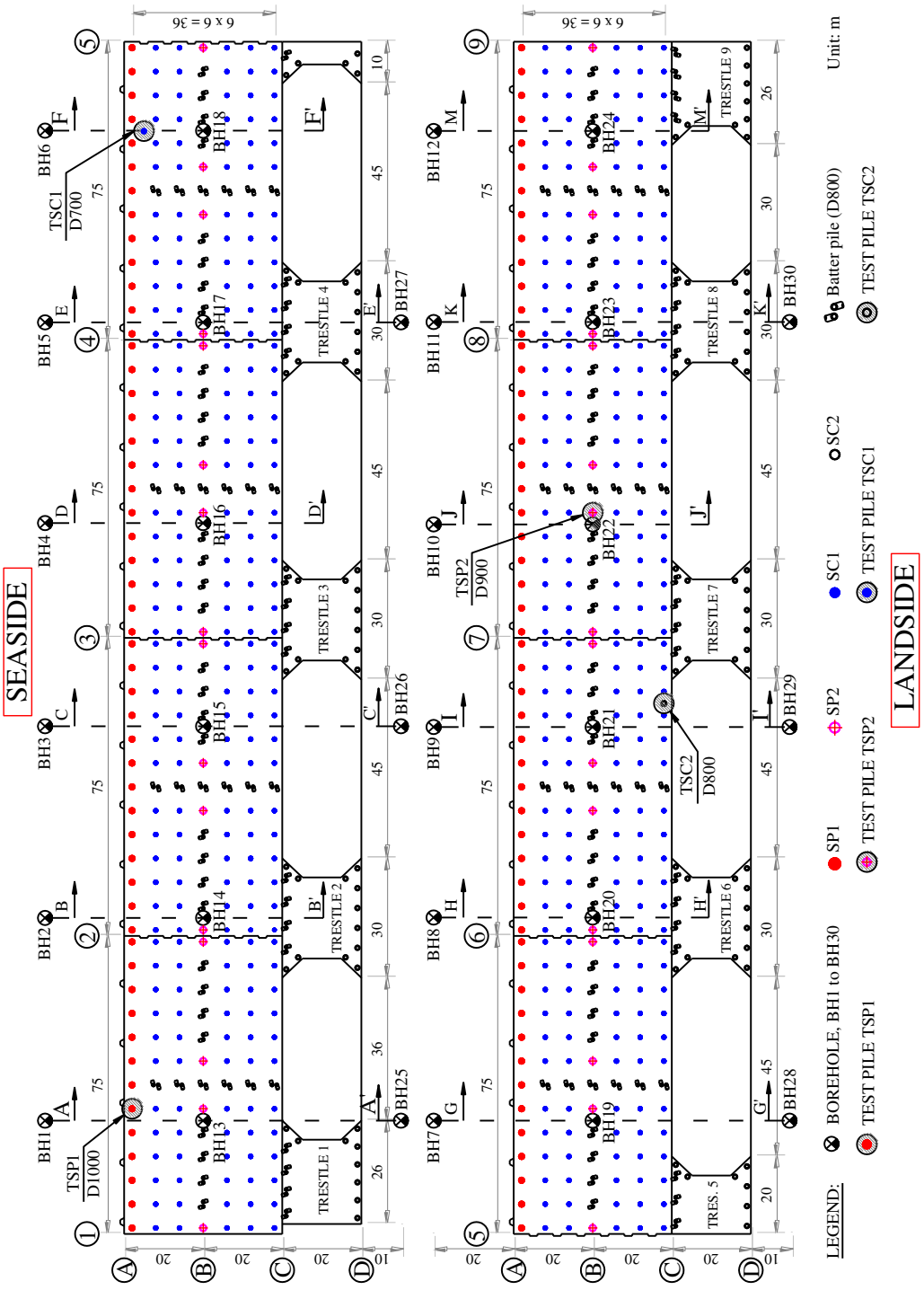

Figure 3. Locations of the boreholes, test piles and working piles.

Locations of the boreholes are shown in Fig. 3, together with the locations of the test piles and the working piles. Of the four test piles, only the TSP1 and TSP2 were re-used as working piles. The geological sections of the four test piles are shown in Fig. 4 for the TSP1 and TSC1 and in Fig. 5 for the TSC2 and TSP2. Note that the high water level (HWL), mean water level (MWL) and low water level (LWL) using the Vietnamese national standard elevation system are +3.97 m, +2.67 m and +0.58 m, respectively. The elevation of the working floor of the berth structure is +5.50 m.

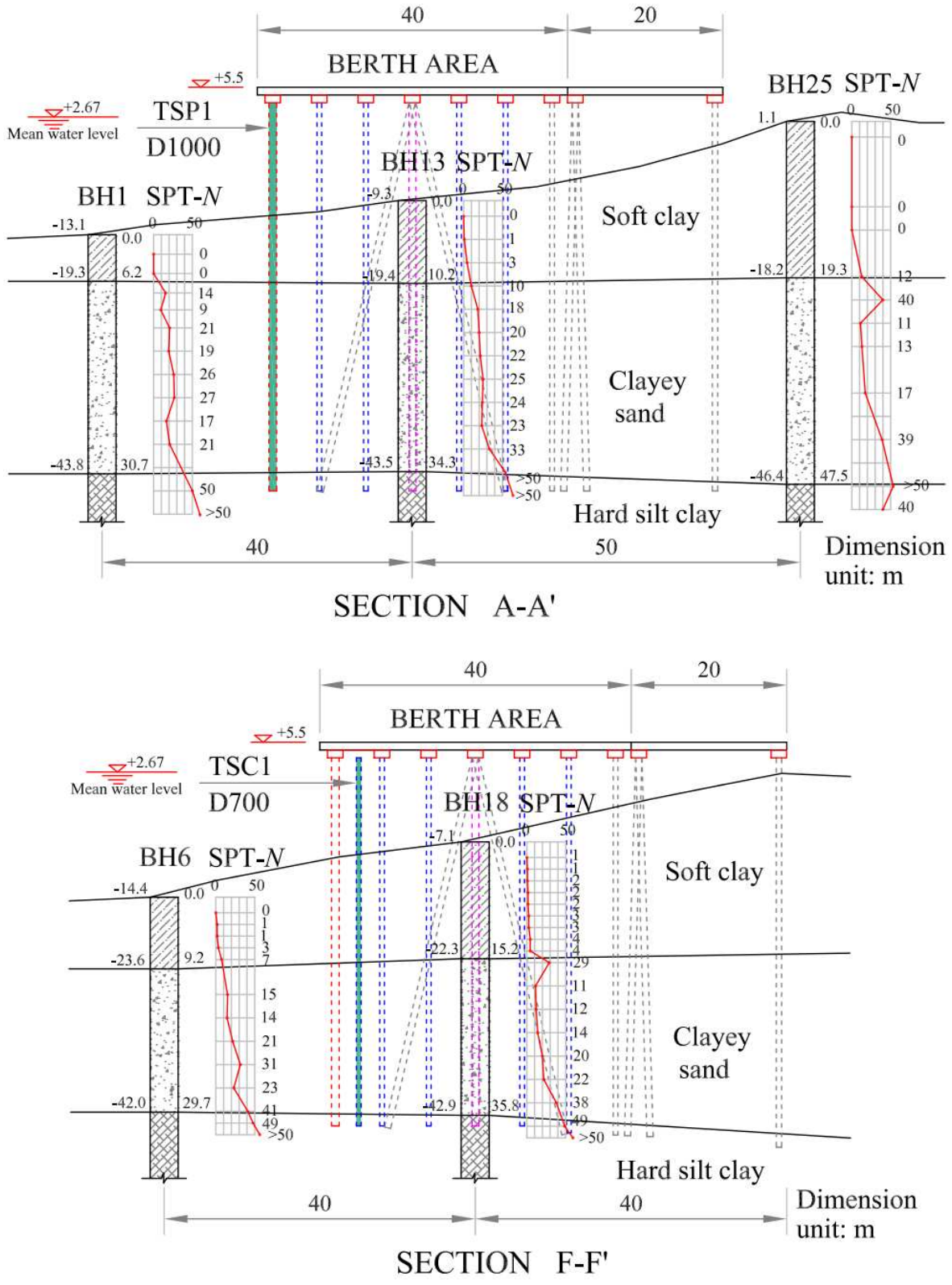

Figure 4. Geological sections at locations of the test piles: (a) TSP1. (b) TSC1.

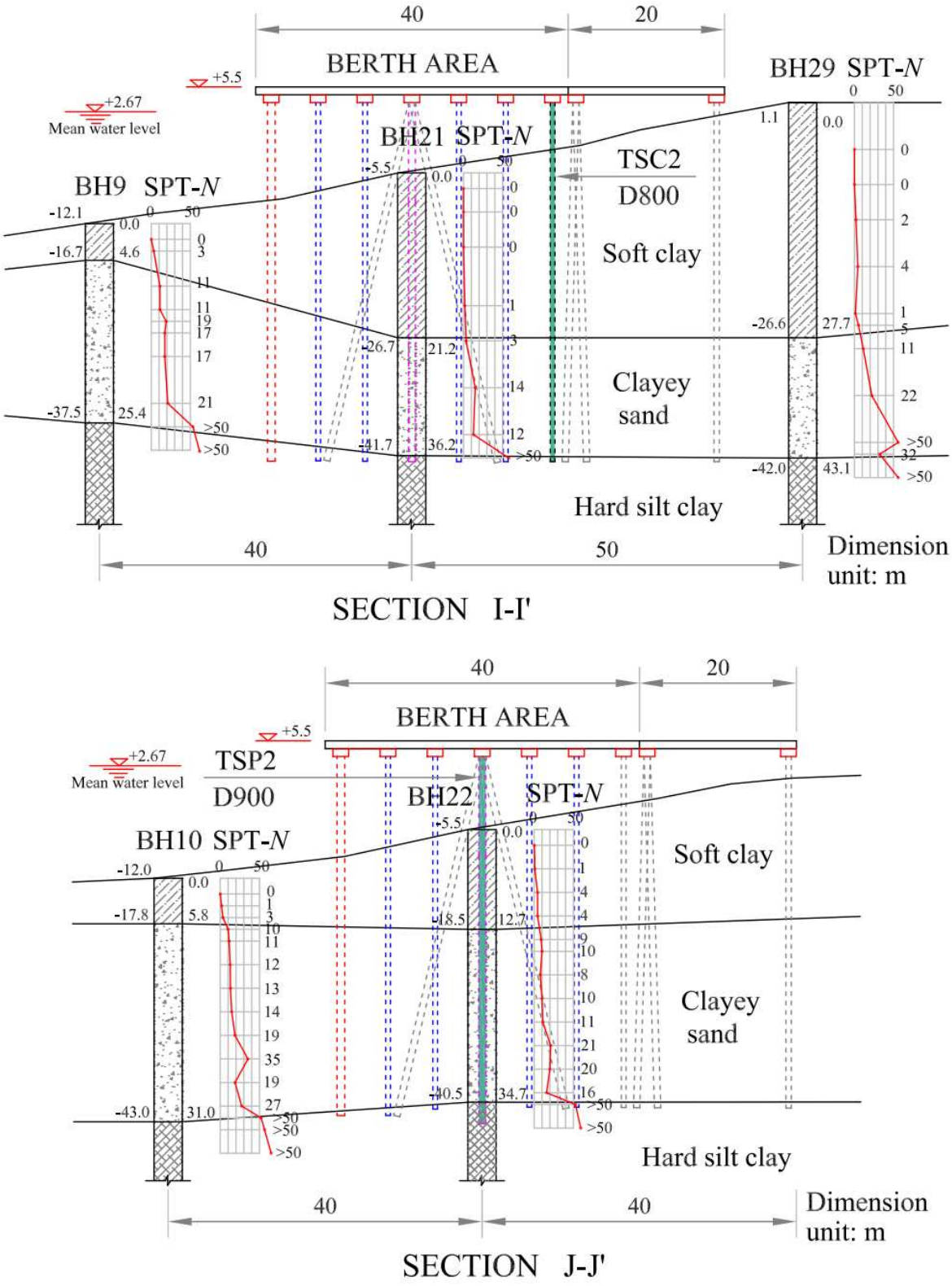

Figure 5. Geological sections at locations of the test piles: (a) TSC2. (b) TSP2.

Estimation of the shear modulus of the ground

The load-displacement relationship of a pile is strongly influenced by the shear moduli of the surrounding ground as well as the distribution of shaft resistance and tip resistance. The shear moduli of the ground needed to be assumed in the WMA of the DLTs of the TSC1 and TSP1. Hence, it was necessary to approximately estimate the shear moduli of the ground at the locations of the test piles.

The soil shear modulus, G_0, at small strain level was estimated using the following empirical equation proposed by Imai (1977), for all soil types.

$$G_0 = 98 \times 120 \times N^{0.737} \quad \text{(kPa)} \tag{1}$$

The distribution of the SPT *N*-value with depth at the location of each test pile was interpolated from the SPT *N*-values of the two nearest boreholes, e.g., the SPT *N*-values at the location of the TSP1 was estimated from those of the two boreholes BH1 and BH13 (see Fig. 4a).

Figure 6 shows the estimated distributions of G_0 with depth at each location of the test piles. These values were used as first-order estimates of the shear moduli in the wave matching analysis of the DLTs.

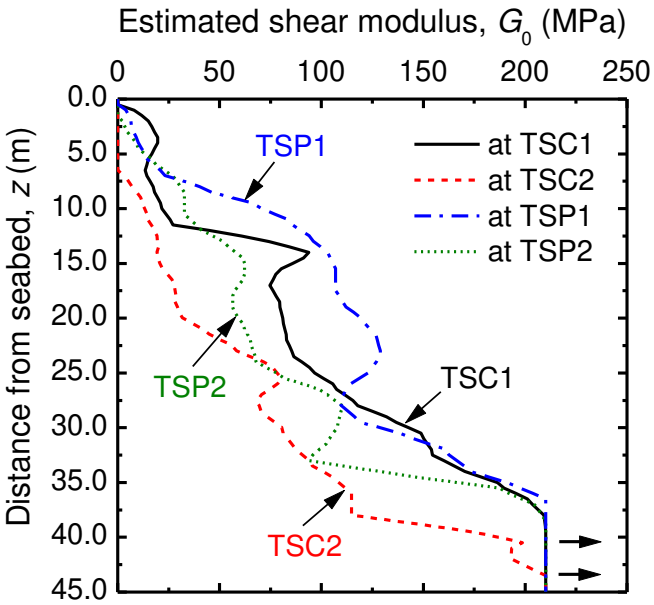

Figure 6. Estimated shear modulus at the four test piles.

Preliminary pile design

Design of the working piles

The berth structure was subjected to various types of loads including vertical loads (self-weight, live load caused by goods) and horizontal loads (earthquake, wind, wave and collision of a ship to the berth structure). Different combinations of loads on the berth structure were considered in preliminary design stage. The maximum compressive force ranged from 1800 kN to 4002 kN, depending on the pile location. Potentially high tensile forces are found at the sea-side row (axis A) and at the middle row (axis B) of the working piles. Hence, the steel piles were used for axes A and B while the concrete piles (spun piles) were used for the remaining locations. Due to the wide range of the pile head force, it was decided to use four pile types which can support the above forces. The location of each pile type is shown in Fig. 3.

The design working vertical load of each pile type is listed in Table 1. Under these loads, the allowable settlements of the piles without taking into account the pile elastic shortening is 20 mm.

According to TCVN 205-1998, the selection of the factor of safety, *FS*, for determining the required capacity depends on the method to estimate the ultimate capacity, Q_u, e.g., *FS* = 2.5 to 3.0 is employed if Q_u is calculated from the empirical equations, *FS* = 3.0 to 6.0 is employed if Q_u is estimated from the driving formulas, and *FS* = 2 can be employed if Q_u is obtained from SLT. In this study, the required capacity was first estimated from the empirical equation to select the embedment pile length, and then the required capacity was confirmed through the static load test. The required capacities of the four test piles in accordance with SLT (*FS* = 2) and without SLT (*FS* = 3) are listed in Table 2.

Table 1. Working load and corresponding allowable settlement.

Pile type	Diameter	Working vertical load	Allowable settlement
	D (mm)	P_a (kN)	S_a (mm)
SC1 (SCP)	700	1800	20
SC2 (SCP)	800	2585	20
SP1 (SPP)	1000	4002	20
SP2 (SPP)	900	3858	20

SPP: Steel Pipe Pile, SCP: Spun Concrete Pile

Table 2. Required capacity.

Pile type	Required capacity (kN)	
	with SLT	w/o SLT
SC1	3600	5400
SC2	5170	7755
SP1	8004	12006
SP2	7716	11574

Design of the test piles

To adapt the requirement of the capacity, the ultimate capacity, Q_u, of the test piles was estimated using the following equation:

$$Q_u = q_{max} A_p + \sum \tau_{max,i} A_{s,i} \quad (3)$$

in which, q_{max} is the maximum base resistance, $\tau_{max,i}$ is the maximum shaft resistance of soil layer i, A_p is the pile tip area with an assumption that perfect plugging occurs at the pile tip, and $A_{s,i}$ is the circumferential area of the pile along soil layer i. According to Vietnamese pile design standard code, TCVN 205-1998, the strength parameters, τ_{max} and q_{max}, can be estimated from SPT N-value using the following empirical equations:

$\tau_{max} = 2N$ (kPa) for sand (limit value = 100 kPa) (4)
$\tau_{max} = c_u$ or $10N$ (kPa) for clay (limit value = 150 kPa) (5)
$q_{max} = 300N_p$ (kPa) for both sand and clay soils (N_p is limited to 50) (6)

where N is SPT N-value of the soil surrounding the pile and N_p is the average SPT N-value of the soil at the pile tip within a range of $4D$ above and $1D$ below the pile tip.

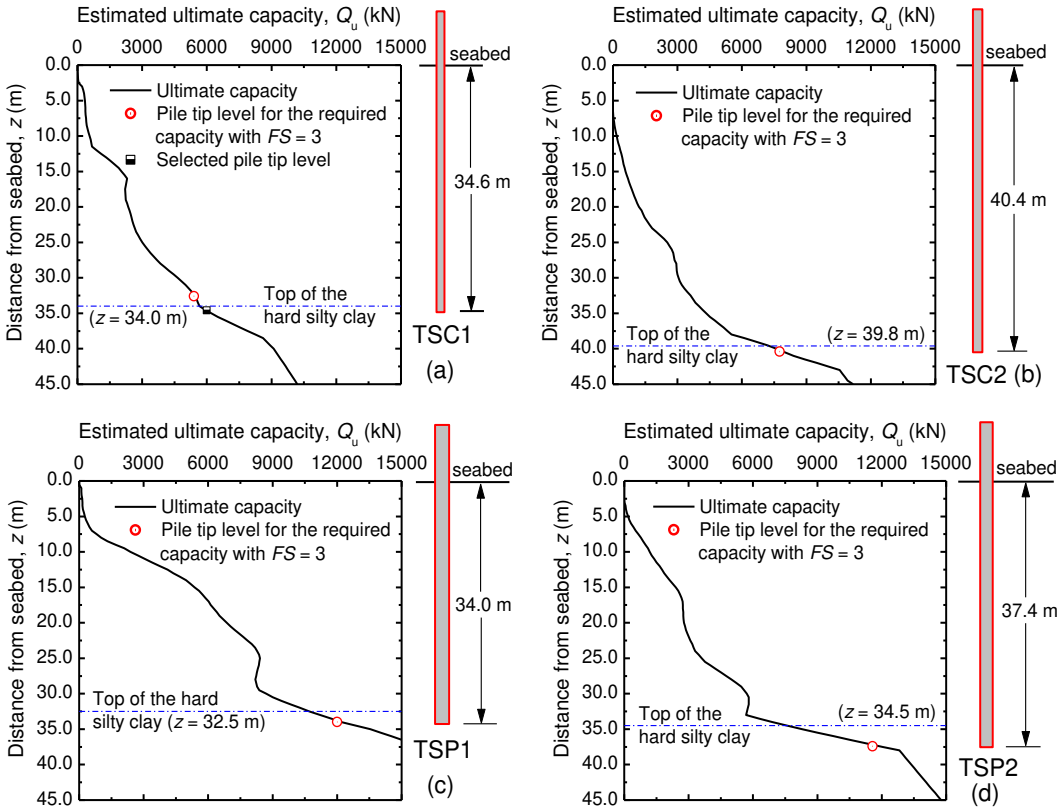

Figure 7. Estimated ultimate capacity with depth and selection of the pile tip level for: (a) TSC1. (b) TSC2. (c) TSP1. (d) TSP2.

Distributions with depth of the ultimate capacity of the test piles are shown in Figs. 7a, 7b, 7c and 7d for the TSC1, TSC2, TSP2 and TSP1, respectively. The required pile tip levels are shown by the red circles in the figures. In case of the TSC1, the required pile tip level does not reach the hard silt clay. However, it was decided to penetrate the pile tip of the TSC1 into the hard silt clay, since TCVN 205-1998 prescribes that the pile tip shall be penetrated at least 0.5 m into a hard bearing stratum. The selected embedment lengths at this preliminary design stage of the test piles were 34.6 m, 40.4 m, 34.0 m and 37.4 m for the TSC1, TSC2, TSP1 and TSP2, respectively. The distance from the seabed to the top level of the test piles (i.e., +6.5 m, 1 m above the working floor of the berth structure) are 15.7 m for the TSC1, 7.5 m for the TSC2, 17.1 m for the TSP1 and 12.5 m for the TSP2. Hence, the minimum length of the TSC1, TSC2, TSP1 and TSP2 are 50.3 m, 47.9 m, 51.1 m and 49.9 m, respectively, as shown in Table 3 along with the other pile specifications.

Table 3. Specification of test piles.

Item	TSC1	TSC2	TSP1	TSP2
Diameter, D (mm)	700	800	1000	900
Wall thickness, t_w (mm)	100	110	12	12
Cross-sectional area, A (mm^2)	188495	238447	37247	33477
Young's modulus, E (kPa)	4.3×10^7	4.3×10^7	2.0×10^8	2.0×10^8
Pile density, ρ (ton/m^3)	2.5	2.5	7.88	7.88
Wave speed, c (m/s)	4148	4148	5038	5038
Minimum pile length, L_{min} (m)	50.3	47.9	51.1	49.9
Allowable compressive stress, σ_{com} (MPa)	64.16	64.16	360	360
Allowable tensile stress, σ_{ten} (MPa)	7.85	7.85	360	360
Allowable compressive force, F_{com} (kN)	12090	15299	13409	12051
Allowable tensile force, F_{ten} (kN)	1480	1872	13409	12051

Test pile driving

In order to drive a pile to the designed depth without any damage to the pile, selecting a pile driving system with adequate energy is very important. This selection involves several factors such as: the size and type of the pile, the properties and topography of the ground, the location of the project (whether driving on land or in water) and the pile driving cost. In order to have an economical and efficient solution when driving a very long pile (L ~ 50 m) with a large diameter (D = 700 to 1000 mm) through a sandy soil of medium density in offshore condition, a diesel hammer was selected for this project. The required energy of the hammer and the driving work of the test piles are presented below.

Selecting the pile driving hammer

According to TCVN 286-2003, the minimum required energy, E_h (Nm), of each blow is estimated based on the following empirical equation:

$$E_h = 1.75 \times a \times P_a \tag{7}$$

in which a = 25 Nm/kN is empirical constant, P_a (kN) is the design working load of the pile.

In case of a single-acting diesel hammer, the hammer mass, M_h (kg), must be consistent with the following conditions:

$$M_h + M_p \le \frac{5E_h}{g} \tag{8}$$

where M_p (kg) is the mass of the pile including masses of the helmet and cushions, and g is the gravity acceleration (= 9.81 m/s^2). It should be noted here that units on the left and right side of Equation 8 are not consistent. Equation 8 is an empirical equation specified in TCVN 286-2003.

Table 4 lists the minimum driving energy and the maximum hammer mass required for the four test piles. From these requirements, a diesel hammer, Delmag D100-13, was selected for the driving work of the test piles. The main specifications of the hammer indicated in Table 5 satisfy the requirements of driving of all the test piles. Selection of the pile driving hammer for the working piles needed to be reconsidered, if the driving stresses

predicted by the wave propagation analysis presented in a later part in this paper exceeded the allowable values of the axial stresses or axial forces of the test piles (see Table 3).

Table 4. Estimation of required energy for pile driving hammer and condition for hammer mass.

Item	TSC1	TSC2	TSP1	TSP2
Design working load, P_a (kN)	1800	2585	4002	3858
Mass of pile, M_p(ton) including helmet and cushions	26.5	32.1	18.2	15.5
Minimum required energy, E_h (kNm)	78.8	113.0	175.1	168.8
Maximum mass of hammer, M_h (ton)	13.6	25.5	71.0	70.5

Table 5. Specification of the pile driving hammer.

Item	Specification
Pile driving hammer	Delmag, D100-13
Hammer mass, M_h (kg)	10000
Drop height of hammer, H (m)	2.8
Energy per blow, E_h (Nm)	213860 to 333540
Number of blows per minute	36 to 45
Suitable for driving pile with mass, M_p, up to (ton)	40

Requirements for driving the test piles

Based on the minimum required pile length, L of about 50 m, the maximum manufactured pile segment length, L_{seg} (not longer than 30 m) as well as transportation limitations, the TSC1 and TSC2 consisted of two segments in which the lower segment is 30 m and the upper segment is 26 m (Fig. 8a). The reason for the longer lower segment is to ensure that the pile tip is driven though the soft clay and is laid in the clayey sand at the end of the driving work of the lower segment. Meanwhile, the test steel pipe piles, TSP1 and TSP2, consisted of three segments with 20 m length for each. Like the above purpose, Seg. 1 and Seg. 2 of the TSP piles were spliced on the barge to form the lower segment of 40 m length (Fig. 8b). The lower and upper segments of all the test piles were welded at the site.

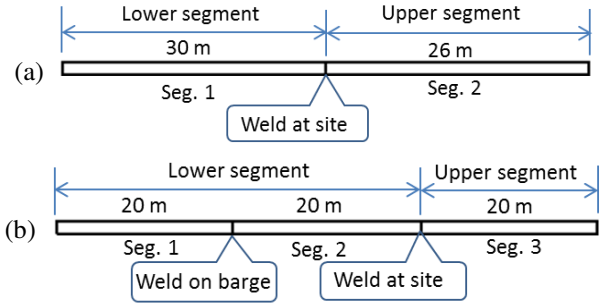

Figure 8. Pile combination from its segments. (a) TSC1 and TSC2. (b) TSP1 and TSP2.

In order to possibly reach the required capacity, the piles have to be driven to the designed depths with an appropriate penetration per blow. According to TCVN 286-2003, when driving a pile using a diesel hammer, the average settlement per blow, S, obtained from the last 10 blows has to be smaller than the required value, S_d, calculated from Eq. (9a). The values of S_d for the four test piles are listed in Table 6.

$$S_d = \frac{e_f M_h g H}{Q_d} - 0.5\sqrt{\frac{2e_f M_h g H L_p}{EA}} \tag{9a}$$

in which: e_f is the hammer fall efficiency, $e_f = 0.8$ for a single-acting diesel hammer.
Q_d is the total dynamic pile resistance which is usually assumed to be equal to the design working load, P_a, with the safety factor of more than 3 for the purpose of driving control. $FS = 4.5$ was chosen for this particular case to ensure pile driving termination.
L_p is the pile length, $L_p = 56$ m for SC piles, $L_p = 60$ m for SP piles.
E is the Young's modulus of the pile material.
A is the net cross-sectional area of the pile calculated from the outer diameter.
H is the falling height of the hammer mass, $H = 2.5$ m for SC piles, $H = 2.8$ m for SP piles.

It is noted that Eq. (9a) can also be used for estimating Q_d during driving. Eq. (9a) is rewritten as:

$$Q_d = \frac{e_f M_h g H}{S_d + 0.5\sqrt{\frac{2e_f M_h g H L_p}{EA}}} \quad (9b)$$

Q_d is calculated using the measured value of S_d during driving by means of Eq. (9b).

Table 6. The maximum settlement per blow of the four test piles.

Item	TSC1	TSC2	TSP1	TSP2
Maximum penetration per blow, S_d (mm)	4.8	2.0	4.7	4.5

The sequence of the driving work of the test piles is as follows:

1. The lower segment is first driven into the ground to the given depth.
2. The welding work of upper and lower segments shall be carried out immediately at the site right after the completion of the driving work of the lower segment.
3. Further driving is conducted as soon as the welding work is completed and approved.
4. The pile is driven to the designed depth with the penetration per blow being smaller than the required value.

Note that, settlement per blow, *S*, and rebound, *R*, was measured at the end of driving manually using "paper and pencil method".

Results of driving work of the four test piles

All the test piles were driven into the bearing stratum of the hard silt clay with final embedment lengths as follows: 34.6 m for TSC1, 41.2 m for the TSC2, 34.9 m for the TSP1 and 37.4 m for the TSP2. The embedment pile length of the TSC1 and the TSP2 were similar to those estimated from the empirical equation, while the penetration length of the TSC2 and the TSP1 were 0.8 m and 0.9 m greater than the expected values, respectively. The average settlement per blow calculated from the last 10 blows of the four test piles, TSC1, TSC2, TSP1 and TSP2, were 2.3 mm, 1.3 mm, 0.6 mm and 1.6 mm, respectively. All these values satisfied the requirements indicated in Table 5. The final embedment pile length of the working piles was decided after analysing the results of the static and dynamic load tests of the test piles.

To prepare for the dynamic load test, except for the TSP1, the other three test piles were cut to the cut-off level, as illustrated in Fig. 9.

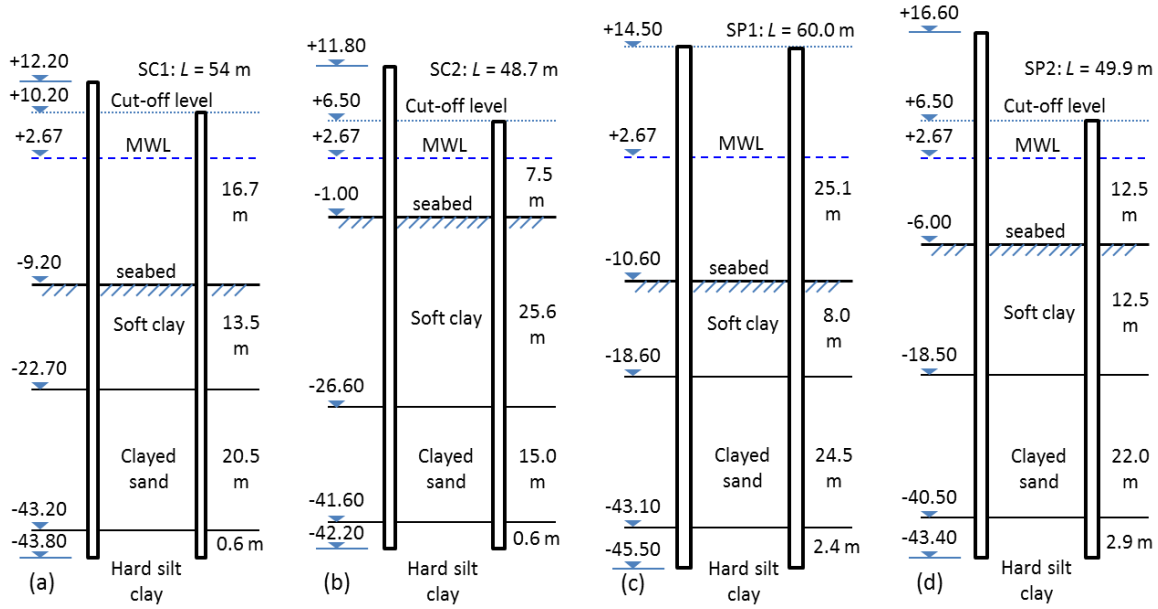

Figure 9. Illustration of the four test piles before and after cutting the pile to the cut-off level. (a) TSC1. (b) TSC2. (c) TSP1. (d) TSP2.

Test procedure

Table 7 shows the testing schedule for each test pile including dynamic load test at the end of the driving work (EOD), dynamic load test at the beginning of re-striking (BOR) after rest period (7 days for the TSC1, 34 days

for TSP1), and static load test after further rest period (10 days for TSC1 and 14 days for TSP1). Static load tests only were carried out for TSC2 and TSP2 after rest periods of 17 days and 27 days, respectively, from the day of driving.

Table 7. Schedule for the test piles.

Test date	TSC1	TSC2	TSP1	TSP2
End of driving, EOD	21-Feb-2011	16-Mar-2011	26-May-2011	7-May-2011
Rest period before re-striking	7 days		34 days	
Beginning of re-striking, BOR	28-Feb-2011	17 days	26-Jun-2011	27 days
Rest period before static load test	10 days		14 days	
Static load test, SLT	10-Mar-2011	2-Apr-2011	13-Jul-2011	3-Jun-2011

Dynamic load tests of TSC1 and TSP1

Dynamic load tests were carried out at the end of driving (EOD) and at the beginning of re-striking (BOR) to investigate the "set-up" phenomenon, to check the driveability of the driving system and to identify the soil parameters. In order to measure the dynamic signals, two strain gauges and two accelerometers were attached to the pile at a distance of 2.7 m for the TSC1 and 3.5 m for the TSP1 from the pile top. At the dynamic measurement location, each pair of strain gauges and accelerometers were attached to the pile at symmetrical positions to the pile centre. The same driving hammer in the stage of driving the test piles was used. Illustration of the driving work in DLT is shown in Fig. 10. Monitoring devices were placed at a distance of about 7 to 10 m from the test pile to minimise the possible influence of the pile response on the measured signals.

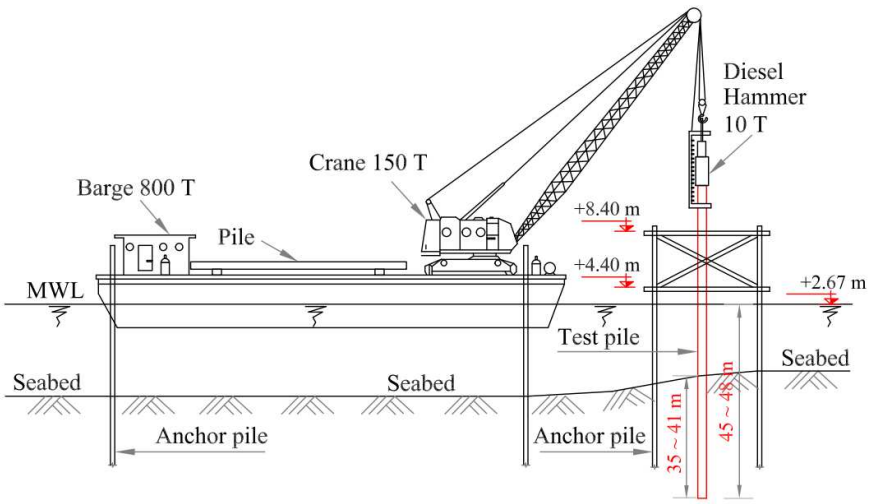

Figure 10. Illustration of the test pile driving by diesel hammer.

Dynamic load tests were conducted in accordance with ASTM-D4945-00 for PDA pile testing using the high strain method. A PDA software suite was used to measure the dynamic signals including strains and accelerations. Using this software, velocity and force signals are automatically obtained from the measured values. The settlement per blow of the pile head was also manually measured at the end of driving.

Static load tests of the four test piles

The static load test was carried out after a given rest period from the BOR test in order to obtain the static load-displacement relation. The maximum load, P_{max}, for each test is listed in Table 8.

Table 8. The maximum test load.

Item	TSC1	TSC2	TSP1	TSP2
Design working load, P_a (kN)	1800	2585	4002	3858
Maximum test load, $P_{max} = 2 \times P_a$ (kN)	3600	5170	8004	7716

Static load tests were conducted in accordance with ASTM-D1143-81 for piles under static axial compressive load. The tests were carried out in offshore condition where the conventional static load test method using steel or concrete blocks as reaction force is very complicated. Hence, the reaction force for these tests was created by 8 anchor steel pipe piles with diameter of 700 mm and 4 pairs of reaction beams, I No. 900, as shown in Fig. 11.

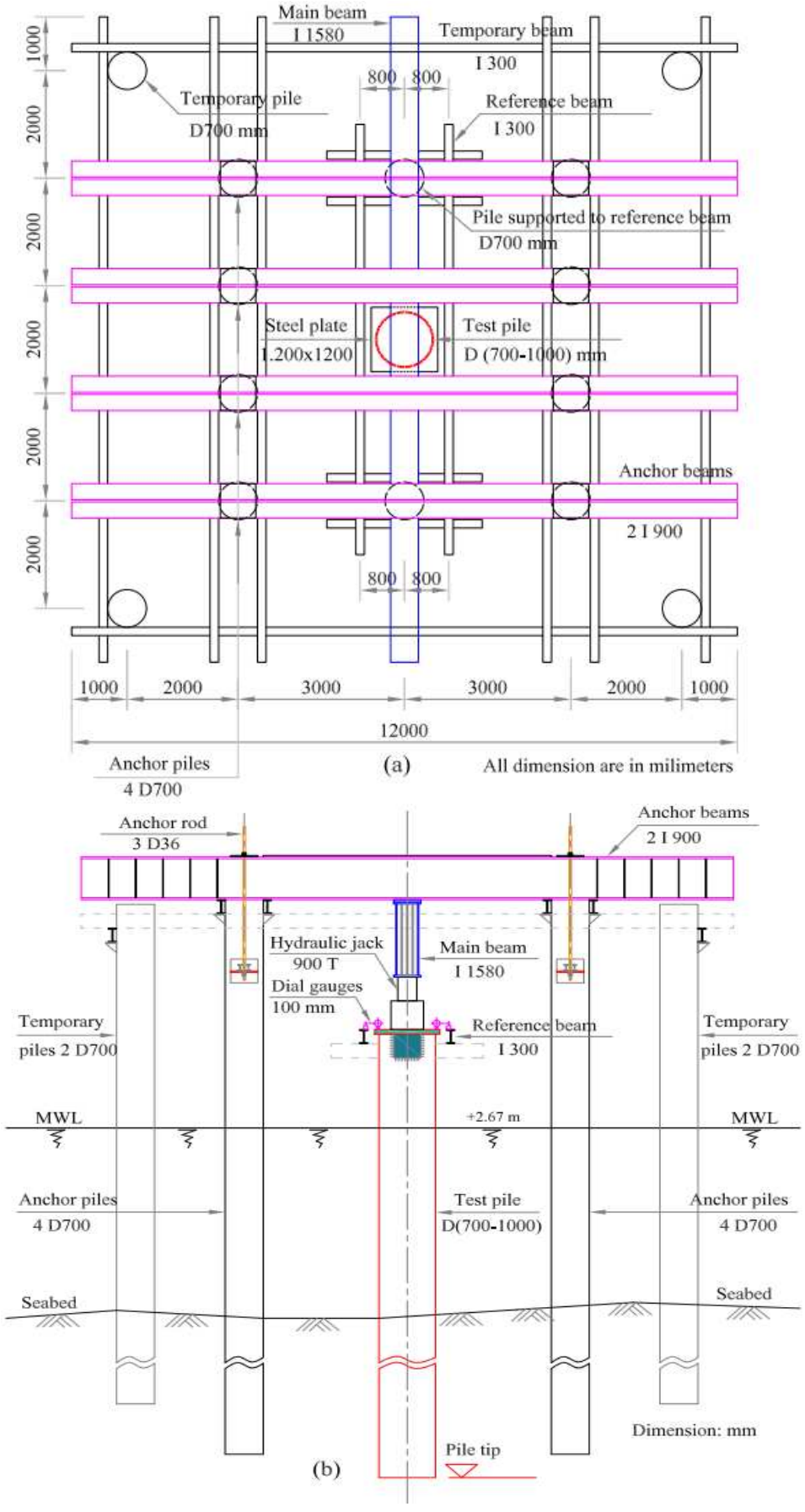

Figure 11. Illustration of the SLT. (a) Layout of the test piles and reaction system. (b) Cross-sectional view of the SLT.

Regardless of the self-weight of the reaction system, reaction anchor piles were designed to have a tension resistance 3 times P_{max}. As the 8 anchor piles were used for the reaction system, each anchor steel pile for SLT of the TSC1, TSC2, TSP1 and TSP2 had to have the uplift capacity of 1350, 1939, 3002 and 2894 kN, respectively. The uplift capacity with depth of the anchor piles at the locations of the test piles calculated from Eq. (3) with an assumption of $q_{max} = 0$, is shown in Fig. 12. The pile tip level for the required uplift capacity is indicated by dot symbol in the figure. The selected pile tip level indicated by triangle symbol corresponding to the embedment length of the anchor piles in SLT of the TSC1, TSC2, TSP1 and TSP2 were 28, 39, 35 and 40 m, respectively. As seen from Fig. 12, the uplift capacities of the anchor piles at the selected pile tip levels are greater than the required capacity. The nearest centre-to-centre distance, L_c, from the anchor piles to the test pile was 3.2 m, corresponding to the ratio L_c/D ranging from 3.2 to 4.6. This distance is large enough to minimise the influence of the anchor pile on the test pile.

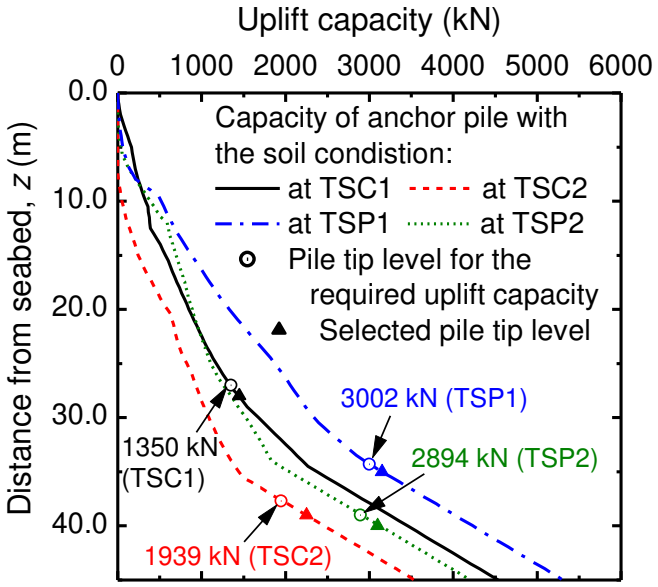

Figure 12. Uplift capacity of the anchor piles with the soil conditions at the TSC1, TSC2, TSP1 and TSP2.

In the static load test, in order to measure the applied force and the corresponding pile head settlement, the testing system consisted of a hydraulic jack with a capacity of 9 MN and 4 dial gauges of 100 mm in range. The jack was placed on the pile top and under the main beam I No. 1580 as shown in Fig. 11b. The dial gauges were placed firmly on two stable reference beams supported by two additional anchor piles to minimise the influences of soil movement and deformation of the equipment on the measurements.

The loading and unloading processes indicated in Fig. 13 were employed in the SLT and include two cycles with 21 steps as follows:

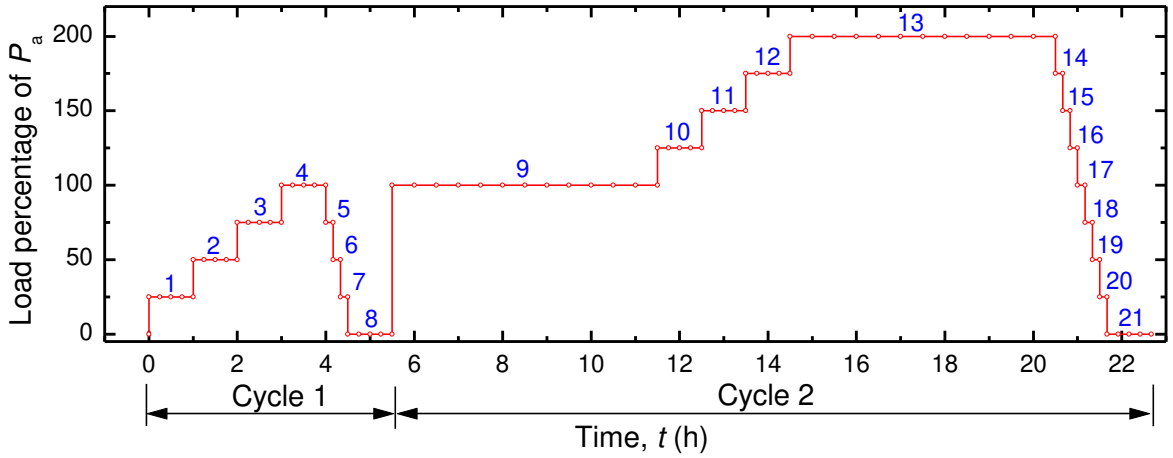

Figure 13. Loading process in SLTs.

1. First cycle (8 steps, from step 1 to step 8): Loading to the design working load, P_a, then unloading to zero. Increment of the applied load at each loading step was set at 25% of the design working load. Load maintaining time of each step was 1 hour. Each unloading step was the same as that in the loading step and the load maintaining time of each step was 10 minutes.

2. Second cycle (13 steps, from step 9 to step 21): After 1 hour of unloading to zero in the 1st cycle, reloading to the design working load and maintaining the load for 6 hours at step 9. Further load was applied until the maximum load, P_{max}. At the maximum load, the load maintaining time was also 6 hours at step 13, and thereafter unloading procedure similat to the 1st cycle was used to unload to zero.

For measuring the pile head displacement, after every 15 minutes in loading process and 10 minutes in unloading, the settlement of the pile was recorded.

The pile is considered to reach the failure (ultimate) state if one of the followings occurs:

1. Under the working load, the pile displacement without taking into account the pile compression exceeds 20 mm.
2. When unloading the working load to zero, the residual settlement exceeds the limit value, S_{ar} = 10 mm.
3. Under the maximum load, the total displacement of the pile head including the pile compression exceeds 10% of the pile diameter.
4. During the test, the pile is found to be away from its original position or to be damaged.

The first criterion can be expressed by means of the allowable pile head displacement including the pile compression under the working load. In accordance with TCVN 269-2002, the elastic pile compression, ΔL, of a friction pile with a length, L, subjected to a vertical pile head load, P, can be calculated using the following equation:

$$\Delta L = \frac{2}{3}\frac{PL}{EA} \tag{10}$$

in which E and A are the Young's modulus and cross-sectional of the pile, respectively.

The elastic shortening of the pile and the corresponding allowable pile head displacements under the working load, and the allowable pile head displacement under the maximum test load are listed in Table 9.

Table 9. Elastic shortening of the pile and the allowable pile head displacements.

Item	TSC1	TSC2	TSP1	TSP2
Pile compression, ΔL(mm) at working load P_a	8.4	9.3	18.6	18.2
Allowable pile head settlement S_a(mm) with taking into account the elastic shortening of the pile subjected to the working load P_a	28.4	29.3	38.6	38.2
Allowable pile head settlement S_{max}(mm) with taking into account the elastic shortening of the pile subjected to the maximum test load P_{max}	70.0	80.0	100.0	90.0

Results of the static load test will be presented later along with the results of WMA.

WAVE MATCHING ANALYSIS AND TEST RESULTS

Wave matching procedure

Numerical approach

The numerical approach for the analyses of the dynamic load tests is briefly presented. Fig. 14a shows the numerical model used. In this model, the pile and the soil plug are modelled as a series of massless linear springs with discrete masses at nodes. Soil surrounding the pile and beneath the pile tip are taken into account using the rational soil models proposed by Randolph and Deeks (1992).

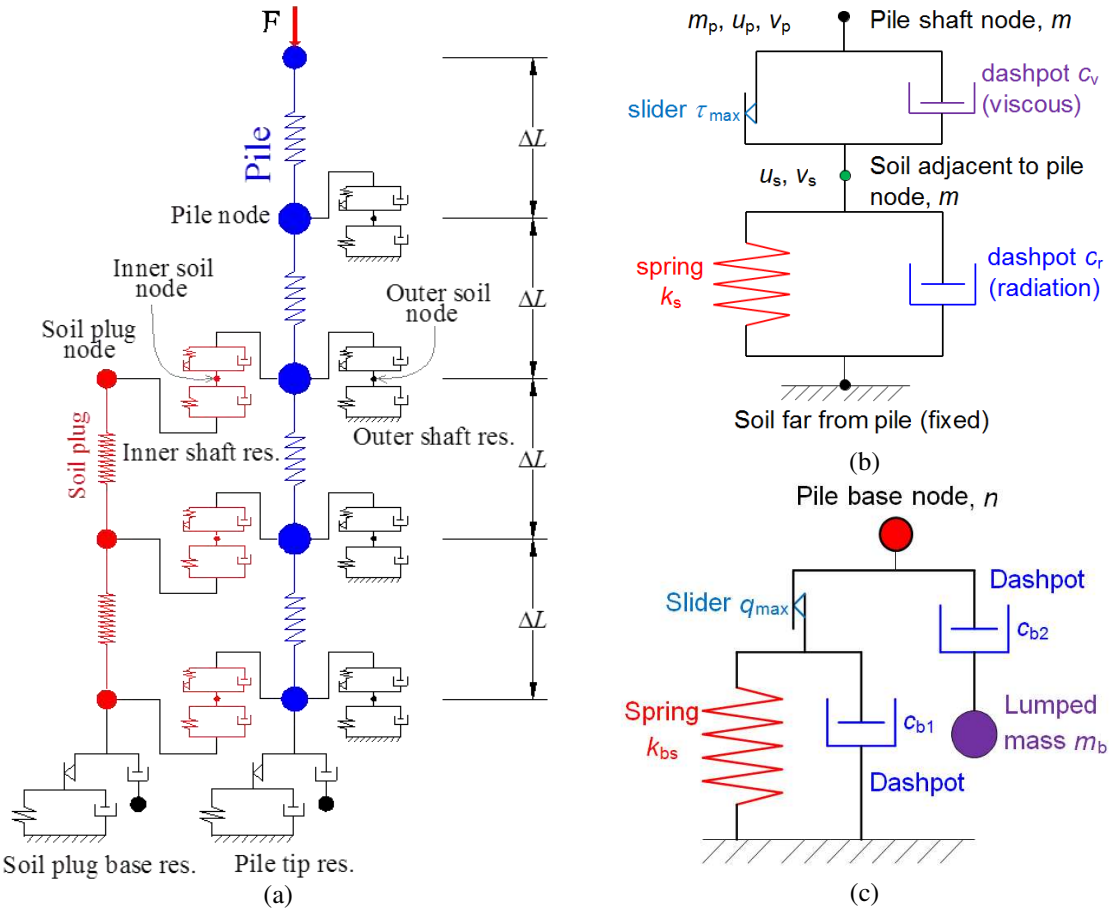

Figure 14. Numerical modelling. (a) Pile – soil system. (b) Shaft soil resistance model. (c) Base soil resistance model.

The soil resistance parameters of the rational soil models shown in Figs. 14b and 14c are approximately related to the soil properties and the pile configurations as follows:

spring stiffness of the outer shaft resistance: $k_s = \frac{2.75G}{2\pi r_o}$ (11)

radiation damping of the outer shaft resistance: $c_r = \sqrt{\rho_s G}$ (12)

spring stiffness of the base resistance of the annular pile base: $k_{b\text{-}p} = \frac{4G}{\pi(r_o + r_i)(1-\nu)}$ (13)

spring stiffness of the base resistance of the soil plug: $k_{b\text{-}sp} = \frac{4G}{\pi r_i(1-\nu)}$ (14)

damping of the base resistance of the annular pile and the soil plug: $c_{b1} = c_{b2} = \frac{3.2}{\pi(1-\nu)}\sqrt{G\rho_s}$ (15)

added soil mass at the annular pile base: $m_{bw\text{-}p} = 16(r_o - r_i)\frac{0.1-\nu^4}{\pi(1-\nu)}\rho_s$ (per unit area) (16)

added soil mass at the soil plug base: $m_{bw\text{-}sp} = 16 r_i \frac{0.1-\nu^4}{\pi(1-\nu)}\rho_s$ (per unit area) (17)

In the above equations, G, ν and ρ_s are the shear modulus, the Poisson's ratio and the density of the soil, and r_o and r_i are the outer and inner radii of the pile.

Writing the force equilibrium equation at all the nodes, the motion of the pile and soil plug can be expressed by the well-known matrix form as follows:

$$[K]\{w\}+[C]\{\dot{w}\}+[M]\{\ddot{w}\}=\{F\} \tag{18}$$

in which [K], [C] and [M] are the global stiffness, damping and mass matrices, respectively. $\{w\}$, $\{\dot{w}\}$, $\{\ddot{w}\}$ and $\{F\}$ are the displacement, velocity, acceleration and the applied force vectors, respectively.

The Newmark's β method (1959) in which $\beta = 1/6$ is used to solve the incremental form of the above equation. Note that [K] and [C] matrices are updated in each calculation step while [M] matrix remains unchanged. If the values of [C] and [M] are set to be zero, the above approach can be applied to the static problem.

The details and numerical validation of the proposed method can be found in Phan et al. (2012).

Modelling of the test ground and the pile

Figures 15 and 16 show the profiles of SPT N-values, the soil stratification, location of the pile and the distributions with depth of the shear moduli, G_0, and shear resistances, τ_{max}, for the TSC1 and TSP1, respectively. Note that the values of G_0 and τ_{max} are the first assumption of the soil properties for both the outer and inner soils in the wave matching analysis. Although the 3-layer ground at both the test piles was divided into 5 sub-layers in the analysis, the test pile TSC1 with the length of 54 m was divided into 54 elements and the test pile SP1 with the length of 60 m was divided into 60 elements. Because the top level of the soil plug was not measured during driving, the soil plug height was assumed to be 70 % to 80 % of the embedment pile length. This assumption is reasonable based on research of Paik et al. (2003) and Paikowsky et al. (1989). Hereafter, the distance from the seabed to the top of the soil plug was assumed to be 9 m for the TSC1 and 7 m for the TSP1. The influence of the soil plug height on the wave matching analysis results is discussed later.

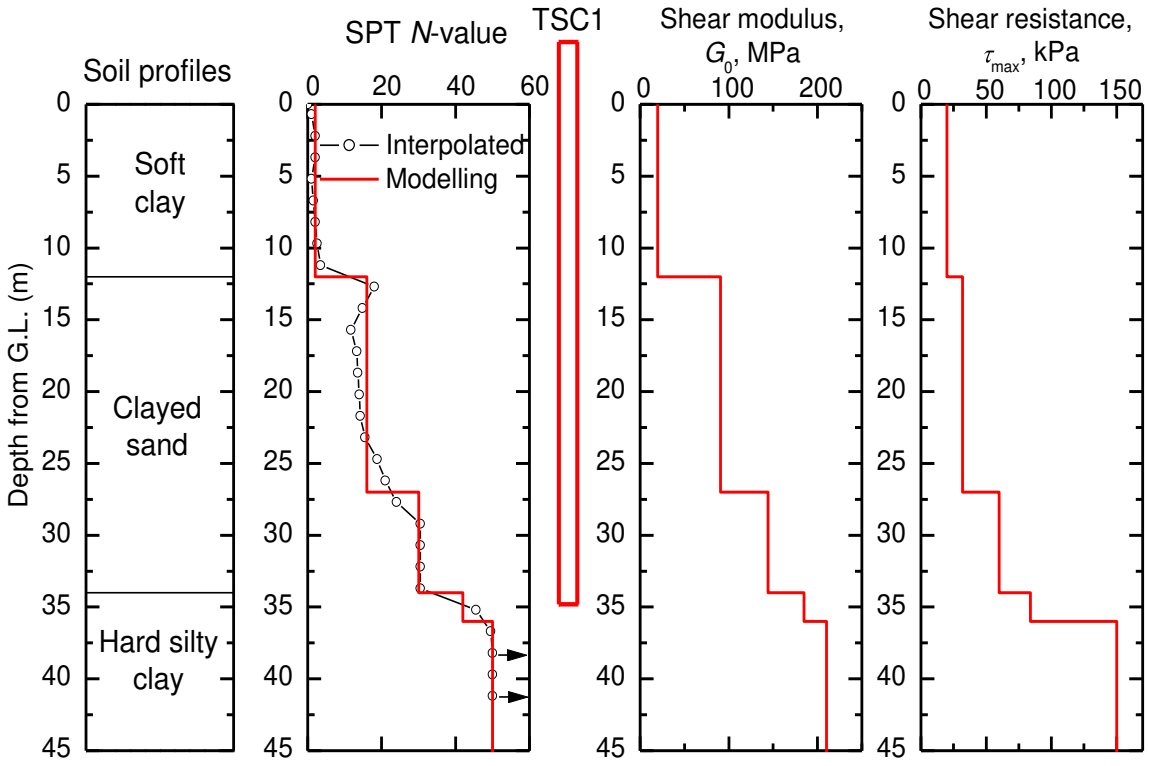

Figure 15. Modelling of the test ground at the test pile TSC1.

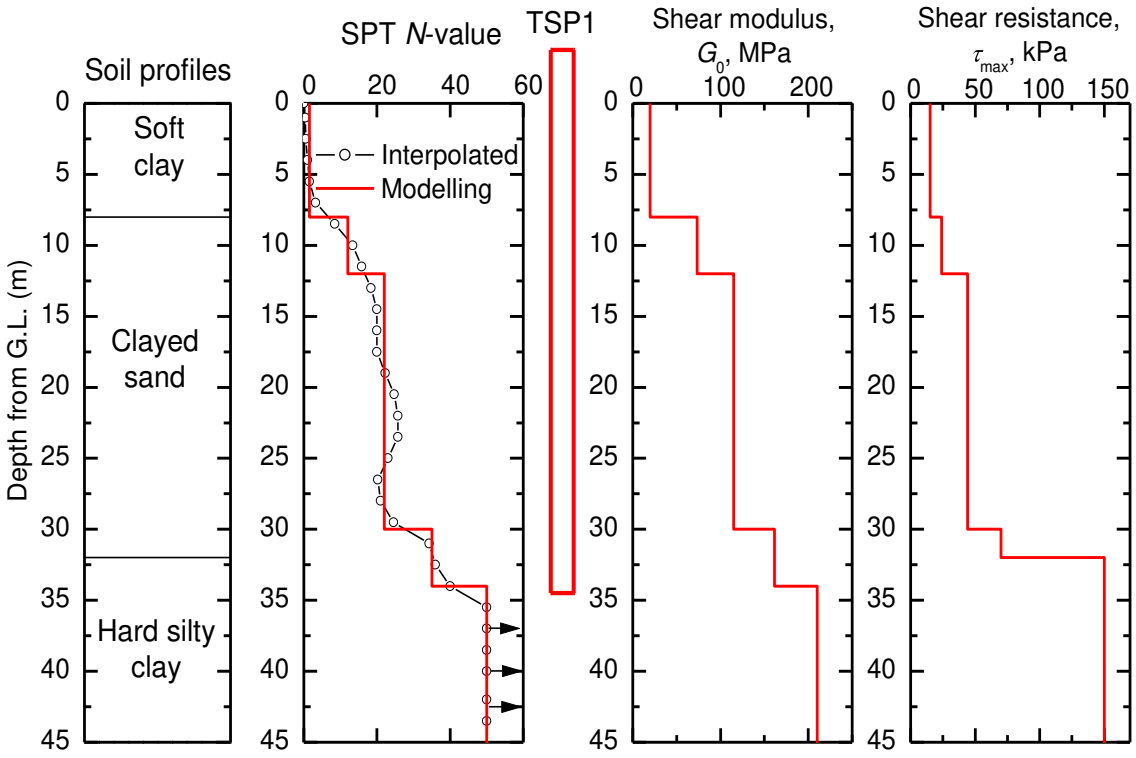

Figure 16. Modelling of the test ground at the test pile TSP1.

The impact head force, $F(0,t)$, is calculated from the measured downward travelling force, $F_{\mathrm{d}}(L_{\mathrm{m}},\ t)$, and the upward travelling force, $F_{\mathrm{u}}(L_{\mathrm{m}},\ t)$, based on the one-dimensional stress-wave theory, as follows:

$$F(0,t) = F_{\mathrm{d}}(L_{\mathrm{m}}, t + L_{\mathrm{m}}/c) + F_{\mathrm{u}}(L_{\mathrm{m}}, t - L_{\mathrm{m}}/c) \tag{19}$$

in which $F_{\mathrm{d}}(L_{\mathrm{m}}, t + L_{\mathrm{m}}/c)$ and $F_{\mathrm{u}}(L_{\mathrm{m}}, t - L_{\mathrm{m}}/c)$ are calculated from the measured force, F_{meas}, and the measured velocity, v_{meas}, as the following equations:

$$F_{\mathrm{d}}(L_{\mathrm{m}}, t + L_{\mathrm{m}}/c) = \frac{1}{2}\left\{F_{\mathrm{meas}}(L_{\mathrm{m}}, t + L_{\mathrm{m}}/c) + \frac{E}{c} v_{\mathrm{meas}}(L_{\mathrm{m}}, t + L_{\mathrm{m}}/c)\right\} \tag{20}$$

$$F_{\mathrm{u}}(L_{\mathrm{m}}, t - L_{\mathrm{m}}/c) = \frac{1}{2}\left\{F_{\mathrm{meas}}(L_{\mathrm{m}}, t - L_{\mathrm{m}}/c) - \frac{E}{c} v_{\mathrm{meas}}(L_{\mathrm{m}}, t - L_{\mathrm{m}}/c)\right\} \tag{21}$$

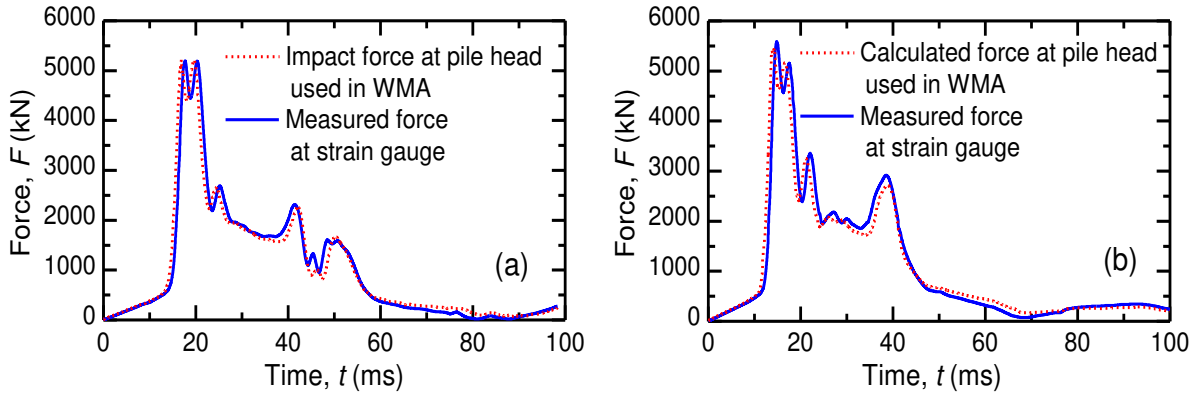

Figure 17. Calculated impact forces at the pile head, together with measured forces of the TSC1 at (a) EOD. (b) BOR.

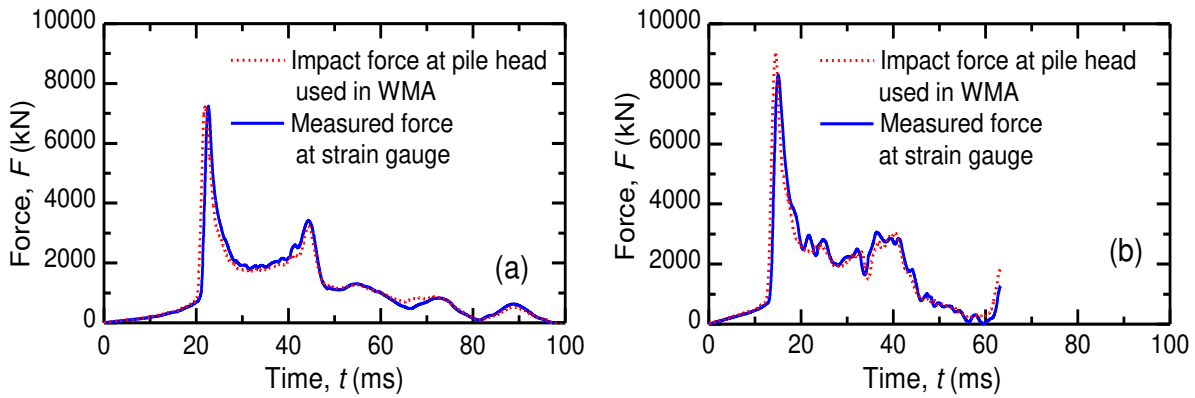

Figure 18. Calculated impact forces at the pile head, together with measured forces of the TSP1 at (a) EOD. (b) BOR.

The calculated impact forces at the pile head in the EOD and BOR tests are shown in Figs. 17a and 17b for TSC1 and in Figs. 18a and 18b for TSP1. The measured forces at the strain gauge level are also shown in the figures for comparison.

Results of wave matching analyses

Results of the TSC1

Under the impact force caused by a hammer mass of 10 ton with a falling height of 2.5 m, the measured settlement per blow of the pile head were 2.3 mm in the EOD test and 1.5 mm in the BOR test. These values along with pile axial force, downward and upward traveling forces, velocities and displacements obtained from the measured dynamic signals at the strain gauge level were used as targets in the wave matching analysis (WMA). In the WMAs, the distributions of the shear modulus of the soil, the outer shaft resistance, the inner shaft resistance, the pile tip resistance and the soil plug base resistance were assumed, because the other soil resistance parameters are estimated from the assumed values of the shear modulus and the pile dimensions (refer to Eqs. (11) through (17)). As for the density, ρ_s, and the Poisson's ratio, ν, of the soils, it was assumed that ρ_s = 17 ton/m^3 and $\nu = 0.3$.

As mentioned earlier, the distance from the seabed to the top of the soil plug was assumed to be 9 m for the TSC1. In the first WMA with the soil properties shown in Fig. 15, good matching was not obtained. Then, the soil properties were changed until good matching between the calculated and the measured responses was observed. The results of the final WMA for both the EOD and BOR tests are shown in Figs. 19 and 20, respectively.

Note that, the calculated downward and upward travelling forces shown in Figs. 19b and 20b were calculated from the calculated axial force, F, and the calculated velocity, v, at the strain gauge level using Eqs. (13) and (14), respectively.

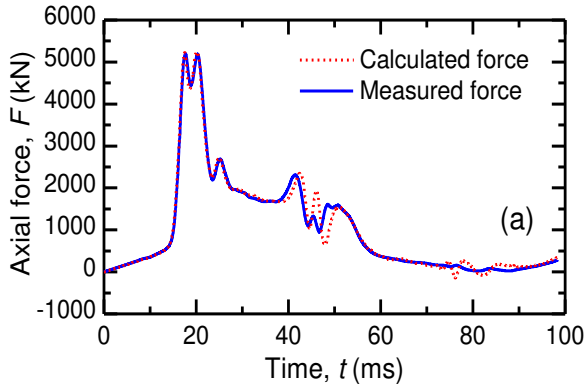

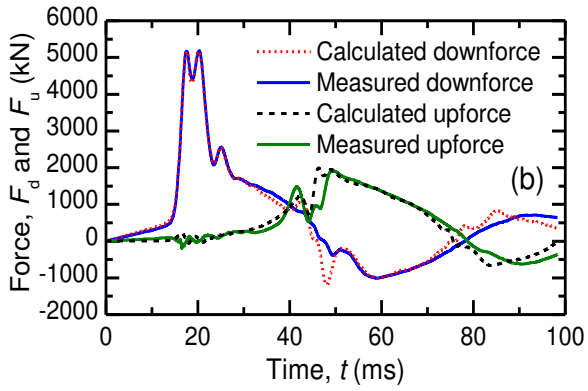

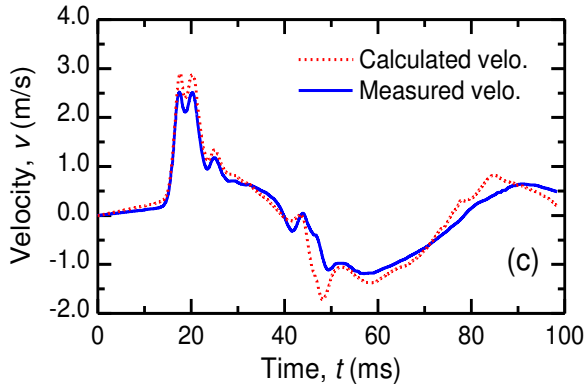

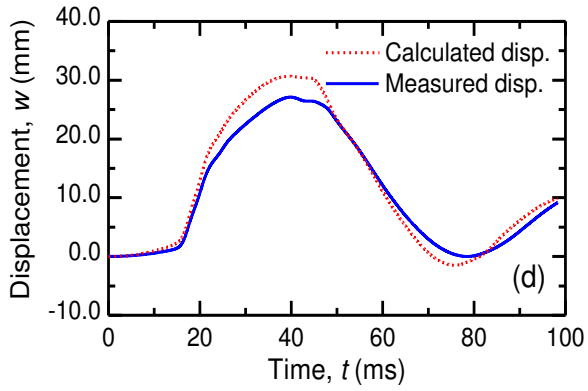

(a) Force. (b) Downward and upward travelling forces. (c) Velocity. (d) Displacement.

Figure 19. Results of the final wave matching analysis of EOD test of the TSC1.

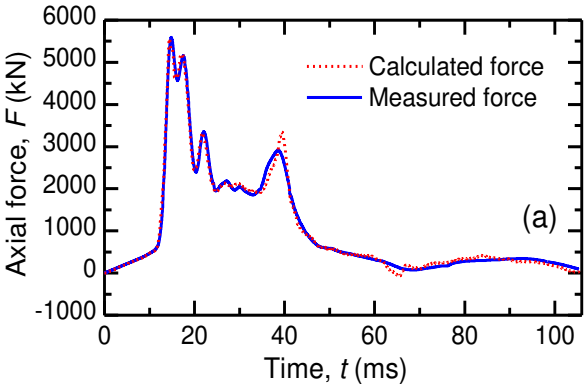

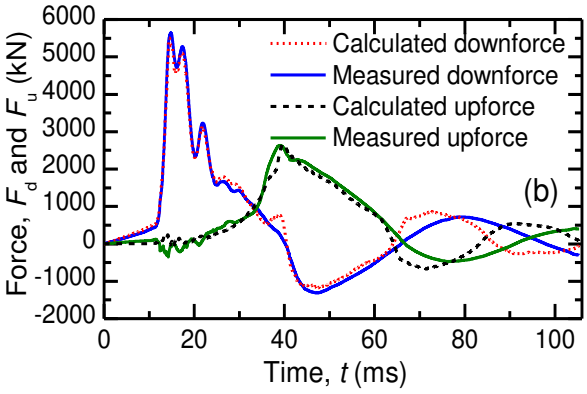

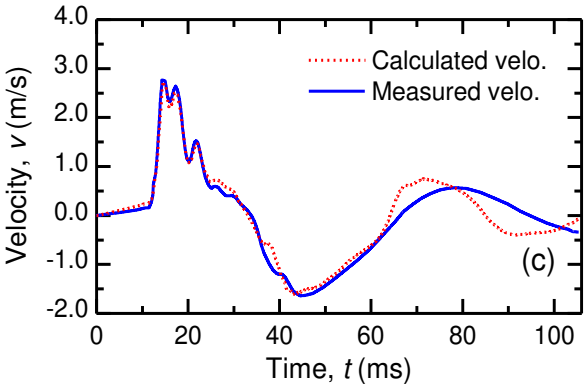

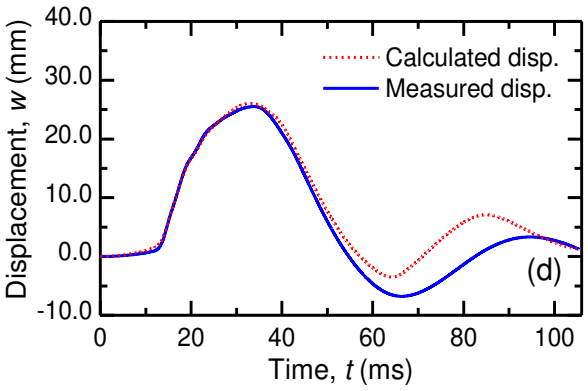

Figure 20. Results of the final wave matching analysis of BOR test of the TSC1.

As seen from the figures, the analysed results of the final WMA are comparable with the measured values for both the EOD and BOR tests. The return travelling time of stress wave in the pile is about 26.0 ms ($2L/c$ = 0.0260 s). The rise time of the axial forces was 17.5 ms in the EOD test and 14.5 ms in the BOR test. Therefore, the peak of the force was reflected at the pile tip and returned to the strain gauge level at t = 43.5 ms (26 + 17.5 ms) in the EOD test and at t = 40.5 ms (26 + 14.5 ms) in the BOR test. From Fig. 20a, the axial force at the instant of 40.5 ms obtained in BOR test is substantially greater than that in the EOD test (see axial force at t = 43.5 ms in Fig. 19a), indicating that higher soil resistance was mobilised in the BOR test than in the EOD test due to the "set-up" phenomenon during the rest period between the EOD and BOR tests. Of course, the influence of the soil resistance can be found more clearly when we compare the calculated and measured upward travelling forces as shown in Figs. 19b and 20b. Note that the final calculated pile head displacement in BOR test shown in Fig. 20d was 1.28 mm which was in good agreement with the measured value of 1.5 mm.

The soil properties identified from the final WMA are shown in Fig. 21 for the soil surrounding the pile shaft and in Table 10 for the soil beneath the pile tip and the soil plug base. The soil properties in the first assumption are also indicated for comparison.

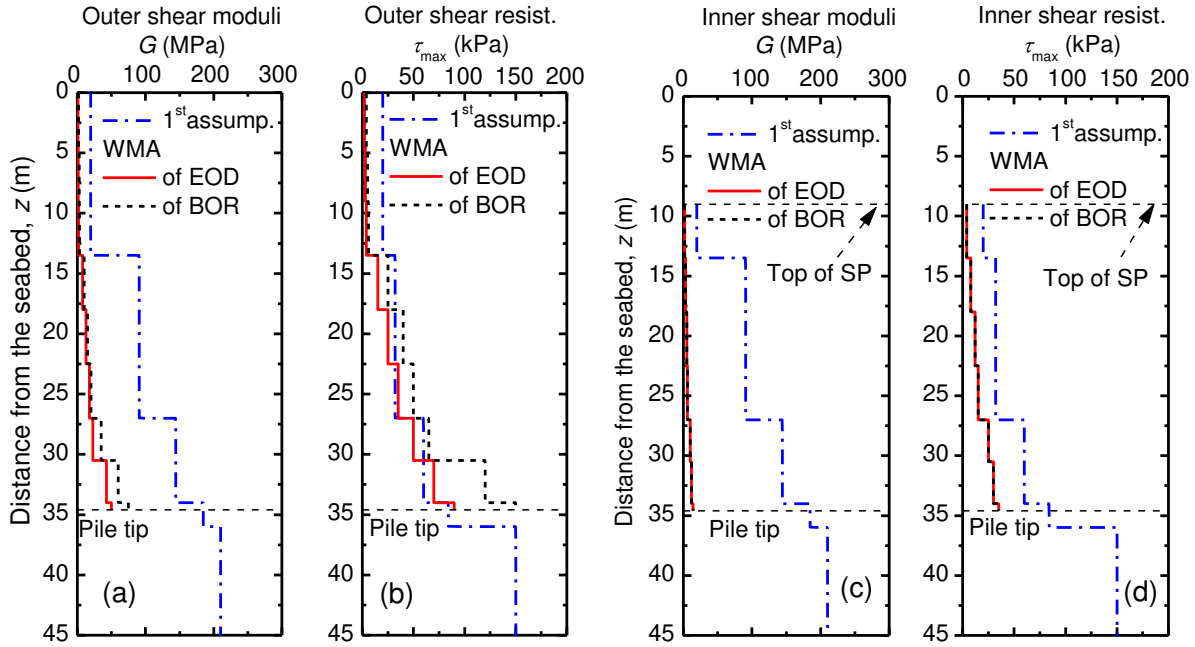

Figure 21. Soil properties obtained from the final WMA of the TSC1 in the EOD and BOR tests.

Table 10. The soil parameters at the pile tip and soil plug base obtained from the final WMA.

Item	Unit	EOD test	BOR test	1st assumption
Shear modulus at the pile tip, G_b	MPa	1700	7000	210
Shear modulus at the soil plug base, G_{sp}	MPa	1000	2000	210
End bearing resistance at the pile tip, $q_{b,max}$	kPa	30700	33500	15000
End bearing resistance at the soil plug base, $q_{sp,max}$	kPa	1000	2000	15000

Figure 21 shows that the values of shear modulus, G, and the shear resistance, τ_{max}, of the soil layers identified from the final WMA of the EOD test are smaller than those of the BOR test, indicating again that the "set-up" phenomenon occurred after the rest period. As seen from the figures, the identified values of G for both tests are smaller than the first assumptions for the soils. The outer shear resistance, however, are smaller than the firstly assumed values for the weak soils (the top soil layer of soft clay and the upper part of the second soil layer of clayey sand with loose packing state). For the harder soils (the lower part of the second soil layer of clayey sand with medium packing state and the third soil layer of hard silt clay), the outer shear resistance identified from the final WMA of the EOD test are comparable with the first assumptions of τ_{max}, but those identified from the final WMA of the BOR test are greater than the firstly assumed values. Comparison of the shear modulus between the identified and the firstly assumed values suggests that reduction factor of 0.1 for soft soils, 0.15 to 0.20 for medium soils and 0.25 to 0.40 for hard soils can be used to estimate the shear moduli of soils at this particular site.

Consideration of the inner soil parameters (τ_{max} and G) was indispensable to get good matching results. The identified inner soil parameters obtained from the final WMA are smaller than both the first assumption and the values of the outer soils. The smaller soil parameter values of the soil plug could be attributed to the soil disturbance when driving the pile in the saturated condition. Furthermore, it could be supposed that the excess-pore water pressure generated in the soil plug during driving was not easy to dissipate after the short rest period.

As for the identified shear moduli and the end bearing resistances of the soil at the pile tip and the soil plug base indicated in Table 10, the values obtained from the final WMA of the EOD test are also smaller than those from the BOR test. For both tests, all the identified values are substantially greater than the firstly assumed values. One reason is that the first assumption of soil parameters were estimated based on the limit of SPT N-values of the soil at the pile tip, $N_p = 50$, which was smaller than the actual value at this site. Another reason might be that the empirical equations are only a crude approach to estimate G and q_{max} for the hard soil beneath the pile tip. Note that the identified end bearing resistance of the soil beneath the soil plug base was substantially smaller than that of the soil below the pile tip. Based on the analysis results, the mobilised inner soil resistances were very small during driving. Hence, the mobilised end-bearing resistance of the soil beneath the soil plug base was limited to a small value.

In order to investigate the influence of the assumed soil plug height on the analysed results, the top of soil plug from the seabed level was varied from 0 to 13 m by examining three more cases (Cases 1 to 3) in which Cases 1 and 2 have higher heights of soil plug while Case 3 has a shorter height of soil plug compared to the previously analysed case (the reference case) with the distance from the seabed to the top of the soil plug of 9 m. The identified soil parameters obtained from the final WMA of the BOR test were used in these analyses. Note that, the inner soil parameters at the top of the soil plug ($z = 9$ m) identified from the final WMA of the BOR test were used for the shallower depths from $z = 0$ to 9 m in Case 1 and Case 2. Results of the pile head displacements obtained from the three additional analyses are compared with that in the final WMA of the BOR test in Fig. 22.

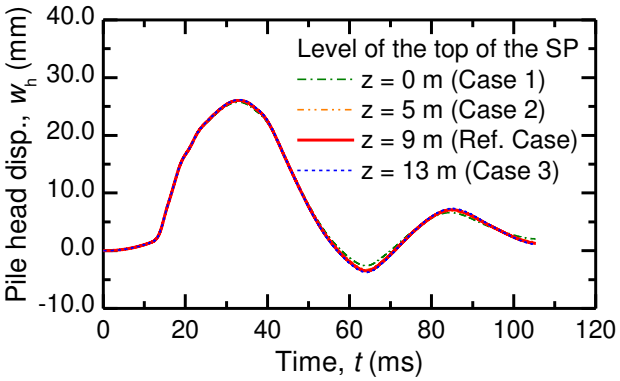

Figure 22. Calculated pile head displacement with different heights of the soil plug.

As seen from the figure, although the soil plug height changed significantly, the calculated result varied slightly, indicating that the influence of the soil plug height in these particular analyses was negligible. One of the reasons could be that the soil near the top of the soil plug was very weak with SPT N-values ranging from 0 to 4 and the identified values of τ_{max} was only 4 kPa for depths from 0 to 13.5 m. Therefore, an assumption of the top of the soil plug height in this study could be acceptable. All of the identified soil parameters were then used to derive the static load displacement curves, as presented later.

Selection of an appropriate pile driving hammer in pile driving is obligatory to ensure that pile is not damaged during driving. In order to evaluate the appropriateness of the selected pile driving hammer, the distributions with depth of the maximum compressive and tensile stresses calculated from the final WMA of the EOD and BOR tests are compared with the allowable values in Fig. 23. It can be seen from the figure that the maximum compressive stress occurred at about 4 m above the pile tip while the tensile stress reached the maximum value at the middle of the embedment pile length. All the calculated stresses in the pile generated during driving were smaller than the allowable stresses, indicating that the selected pile hammer was suitable for the TSC1. Similar evaluation of the suitability to the pile driving hammer is subsequently presented for TSP1.

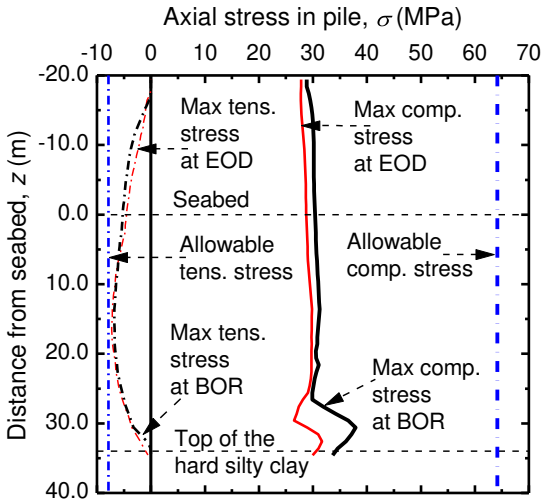

Figure 23. Distribution with depth of the maximum tensile and compressive stresses in the pile during driving of the TSC1.

Figure 24 shows the static load-displacement curves derived from the soil properties identified in the final WMA of the EOD and BOR tests, compared to the static load test result in two cycles of loading process. It should be noted that conducting the SLT just after EOD is not practical (impossible). However, it is interesting to compare the calculated load-displacement curves at EOD and BOD with the measured curve in the SLT to discuss the set-up phenomena of the driven pile.

As seen from the figure, the stiffness of the static response derived from the BOR test is higher than that derived from the EOD test, indicating the "set-up" phenomenon discussed previously. The static response derived from the final WMA of the BOR test is comparable with the SLT, compared to that obtained from the EOD test. As indicated in Table 10, the EOD test was carried out 17 days before the SLT and the BOR test was conducted 10 days before the SLT. The three load-displacement curves in Fig. 24 clearly indicate the "set-up" phenomenon during the period from the EOD test via the BOR test to the SLT. Namely, the soil resistance parameters identified from the final WMAs of the EOD test and the BOD test reflect the effects of generation of excess pore pressures during driving and subsequent dissipation of the excess pore water pressures after EOD, in other words, the change of the effective stresses in the soil surrounding the pile.

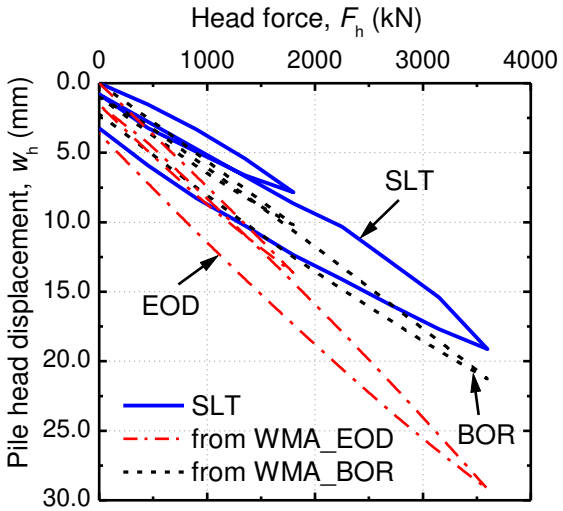

Figure 24. Comparison of the static load displacement curves of the TSC1 (D=700 mm).

From the result of the SLT, the measured settlement S = 9.0 mm at the working load of 1800 kN was sufficiently smaller than the allowable value S_a = 28.4 mm. The measured settlement S = 19.0 mm at the maximum load of 3600 kN was also smaller than 70 mm that is 10% of the pile diameter, and the residual settlement S = 1.0 mm after the full unloading process from the working load was also below the limit value S_{ar} = 10.0 mm. All of these

values indicated that the pile did not reach the ultimate bearing state. Hence, TSC1 has a factor of safety greater than 2 against the working load of 1800 kN.

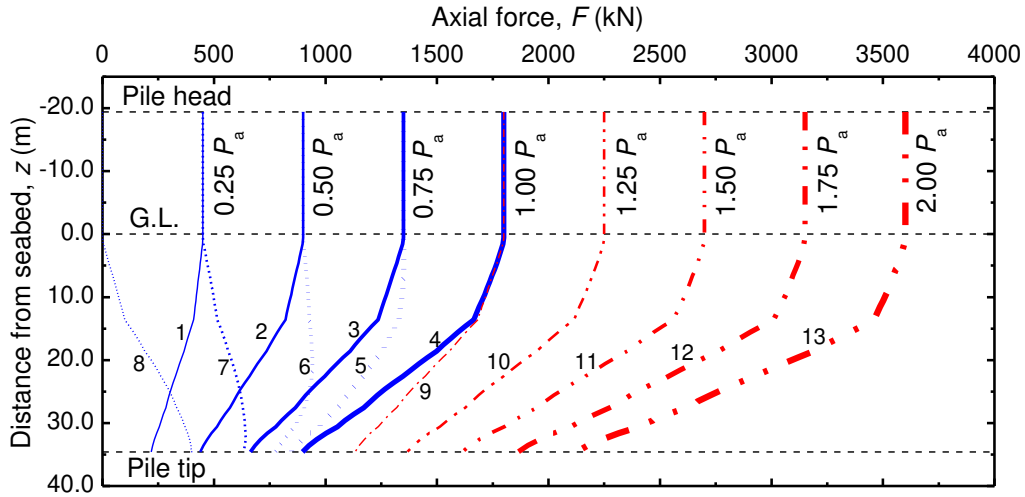

Figure 25. Calculated distributions with depth of the pile axial forces of the TSC1 at the BOR test.

As mentioned earlier, the pile head load and the pile head displacement alone were measured in the SLT. The load-displacement curve derived from the final WMA of the BOR test was comparable with the SLT result (Fig. 24). Therefore, let us discuss more the static response of the TSC1 based on the calculated results of the BOR test including the loading and unloading processes.

Figure 25 shows the calculated changes of distributions with depth of the axial forces in the TSC1, including the first loading process (steps 1 to 4), the first unloading process (steps 5 to 8) and the second loading process (steps 9 to 13, see Fig. 13). The axial force at the pile tip can be regarded as the mobilised pile tip resistance. As seen from the figure, in the first loading process from step 1 to step 4, the mobilised shaft resistance and tip resistance increase with increase in the applied head force. At the working load, P_a = 1800 kN, the mobilised tip resistance, Q_b, and the total mobilised shaft resistance, Q_s, share almost the same force, about 50% of the applied force. When unloading to zero at step 8, axial forces remain along the embedment pile length. These residual forces increase with depth and reach a maximum value of about 400 kN at the pile tip. When reloading to the working load at step 9, the axial forces along the pile deeper than 15 m are greater than those in step 4 because of the residual forces in the pile generated in the previous loading steps. When further loads are applied on the pile head in steps 10 to 13, the mobilised shaft resistance and end-bearing resistance continue to increase, indicating that the pile does not reach the ultimate bearing state at the maximum applied force of 3600 kN.

The TSC1 was not used for the working pile after the completion of the SLT. However, it may be interesting to calculate the pile response, supposing that the TSC1 were loaded to the working load again after the completion of the SLT. For this purpose, the third loading process was fictitiously added to the previous analysis.

Figure 26 shows the calculated distribution of the axial forces in the pile at the end of the third loading process, together with those at the working load in step 4 of the first loading process and in step 9 of the second loading process, and those at the maximum load (step 13) and full unloading step of the second loading process. The figure indicates that when unloading to zero from the maximum load, the residual axial force is again caused along the embedment pile length with a maximum value of 1000 kN at the pile tip which is much greater than 400 kN in the first full unloading step (step 8 in Fig. 25). At the working load, the axial forces decrease with depth in the first and second loading processes, however, the axial force in the third loading process slightly decrease for depths of 0 to 15 m, then increases for depths of 15 to 29 m (neutral plane) and finally decreases with increasing depth. It is clearly seen from comparison of the axial forces in the pile at the working load in three loading processes that the mobilised shear resistances decrease while the mobilised tip resistances increase with increase in the number of the loading processes. Such aspect should be considered when evaluating the pile capacity after the SLT, because the safety margin of the pile tip resistance decreases with increasing number of loading processes in which magnitude of the maximum applied force increases in each process. This aspect will be discussed again in later part for the TSP1, which was reused as a working pile in this site.

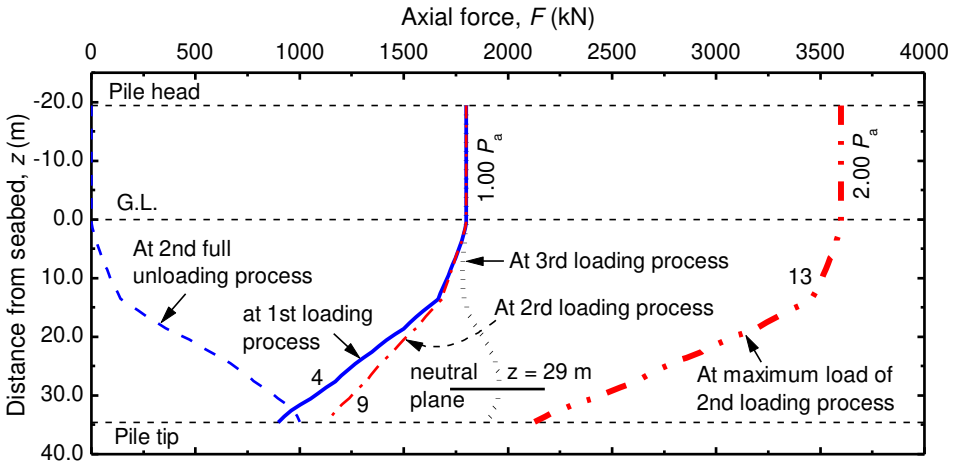

Figure 26. Calculated distributions with depth of the pile axial forces of the TSC1 at the BOR test.

Results of the TSP1

Similar to the TSC1, wave matching analysis was conducted for the TSP1, and the results of the final WMA at the strain gauge level including axial forces, downward and upward travelling forces, velocities and displacements are shown in Fig. 27 for the EOD test and in Fig. 28 for the BOR test. As seen from these figures, the calculated results were comparable with the measured values, when the soil parameters shown in Fig. 29 and Table 11 were assumed.

Note that under the impact force caused by a hammer mass of 10 ton with a falling height of 2.8 m, the measured settlement per blow of the pile head were 0.6 mm in the EOD test and 0.3 mm in the BOR test. As seen from Fig. 28d, the calculated pile head settlement in the BOR test was comparable with the measure value of 0.76 mm.

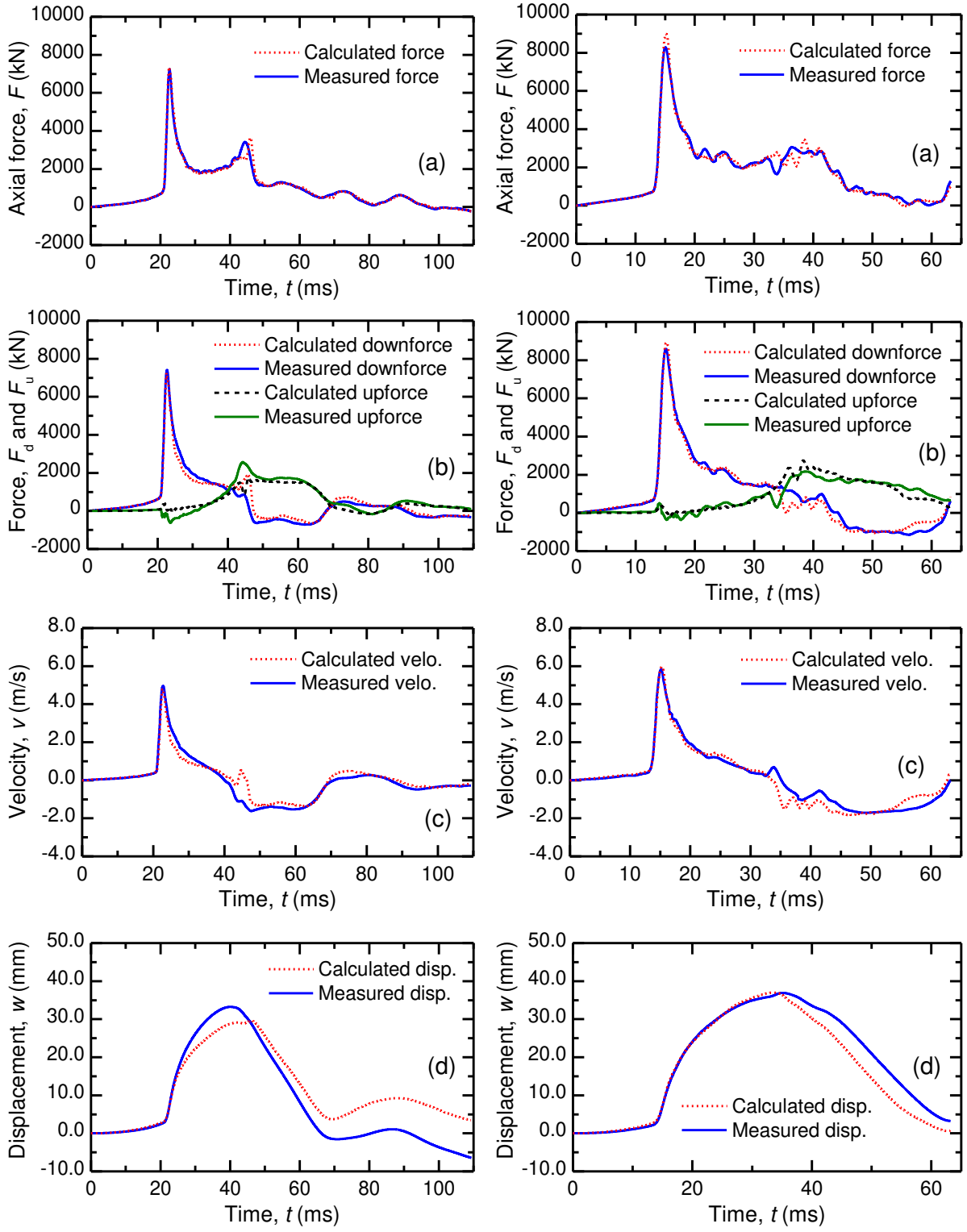

(a) Force. (b) Downward and upward travelling forces. (c) Velocity. (d) Displacement.

Figure 27. Results of the final wave matching analysis of EOD test of the TSP1.

Figure 28. Results of the final wave matching analysis of BOR test of the TSP1.

The soil parameters in the first assumption are also indicated in Fig. 29 for comparison. The values of shear modulus, G, and the shear resistance, τ_{max}, of the soil layers identified from the final WMA of the EOD test were smaller than those from the WMA of the BOR test, indicating again that the "set-up" phenomenon occurred after the rest period. Such phenomenon was also obtained for the soil at the pile tip by comparison of the identified values, G_b and $q_{b,max}$, between the EOD and BOR tests shown in Table 11.

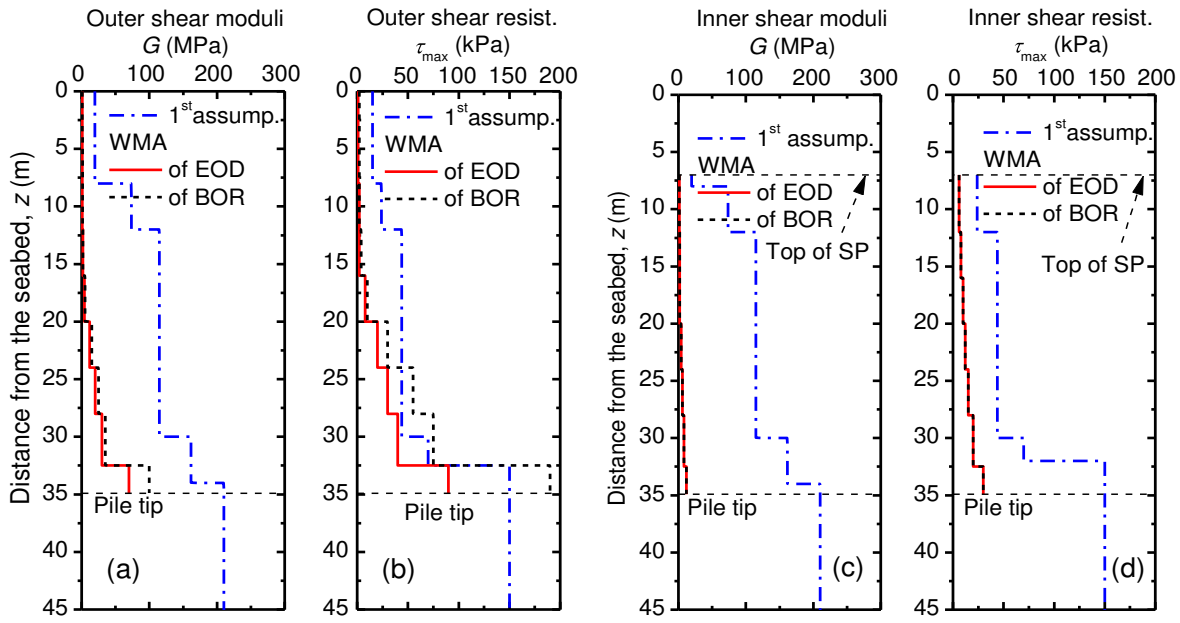

Figure 29. Soil properties obtained from the final WMA of the TSP1 in the EOD and BOR tests.

Table 11. The soil parameters at the pile tip and soil plug base obtained from the final WMA.

Item	Unit	EOD test	BOR test	1st assumption
Shear modulus at the pile tip, G_b	MPa	20000	22000	210
Shear modulus at the soil plug base, G_{sp}	MPa	2000	2000	210
End bearing resistance at the pile tip, $q_{b,max}$	kPa	120000	140000	15000
End bearing resistance at the soil plug base, $q_{sp,max}$	kPa	1000	1000	15000

For the EOD and BOR tests, similar to the case of TSC1, the first assumption of the shear modulus estimated from empirical equation Eq. (1) were overestimated, compared to the finally identified values (Figs. 29a and 29b). For the BOR test, the empirical equations (4) and (5) overestimated the identified shear resistances for the soft soil layers (the first layer of the soft clay and the upper part of the second layer of clayey sand with loose packing state), while underestimated the identified shear resistances for the hard soil layers (the lower part of the second layer of clayey sand with medium packing state and the third layer of hard silt clay).

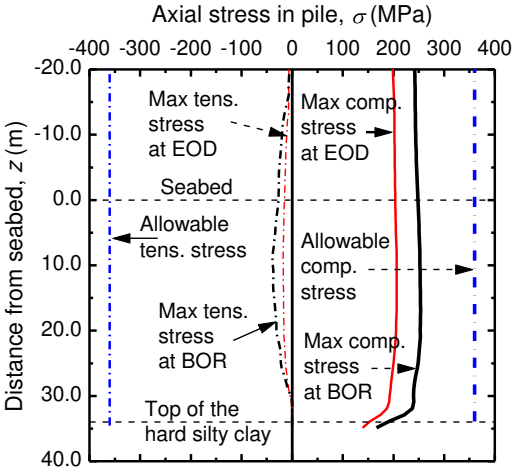

Figure 30. Distributions with depth of the maximum tensile and compressive stresses in the pile during driving of the TSP1.

Let us discuss the suitability of the selected hammer for the TSP1. The calculated maximum compressive and tensile stresses in the pile during driving in the EOD and BOR tests shown in Fig. 30 do not exceed the allowable stresses. Therefore, the selected pile driving hammer is suitable for driving the working piles.

Figure 31 shows the static load-displacement curve derived from the soil properties identified in the final WMA, compared with the static load test result in two cycles of loading process. The stiffness of the static response derived from the final WMA of the BOR test was a little bit higher than that of the static response in the EOD test. Although the rest period between the EOD and the BOR in this test (34 days) was longer than that in the TSC1 (14 days), the difference of the derived static responses between the EOD and the BOR is not remarkable compared to the case of TSC1. Similar to the case of the TSC1, the static response derived from the final WMA of the BOR test was comparable with the SLT result, indicating that the identified soil parameters were reasonable. It is noted that the derived static curve underestimated the measured curve because the "set-up" phenomenon continues for 14 additional days after the BOR test.

According to the final WMA results of TSC1 (Fig. 21d) and TSP1 (Fig. 29d), the set-up phenomena of the inner shaft resistance were negligible in these particular cases. Hence, it could be thought that the set-up phenomena are mainly caused by the set-up of the outer shaft resistance. The different degrees of the "set-up" between the TSC1 and the TSP1 might be explained by the different configurations of the test piles. The TSC1 had an outer diameter of 700 mm and a wall thickness of 100 mm, while the TSP1 had an outer diameter of 1000 mm and a wall thickness of 12 mm (see Table 3). It is reasonable to think that the TSC1 pushed away the surrounding ground outward during driving much more than the case of the TSP1. Hence, greater excess pore-water pressures might have been generated in the ground during driving of the TSC1. If these suppositions are adequate, it is reasonable to state that the TSC1 had a higher degree of the "set-up" phenomenon.

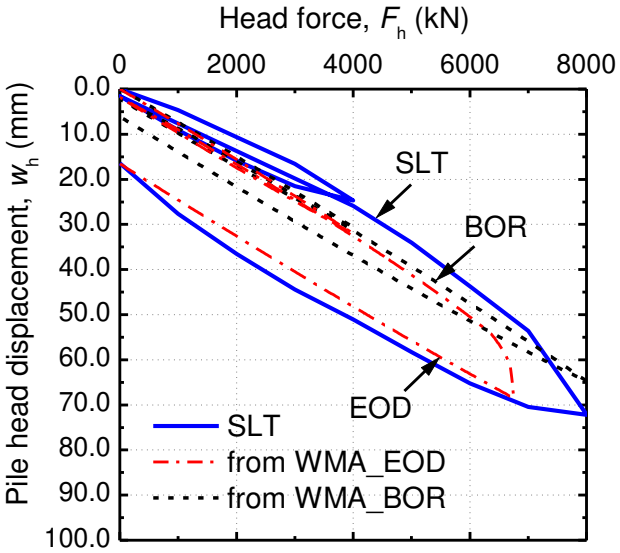

Figure 31. Comparison of static load displacement curves of TSP1 (D=1000 mm)

From the results of the SLT, the measured settlement S = 25.0 mm at the working load of 4002 kN was sufficiently smaller than the allowable value S_a = 38.6 mm. The measured settlement S = 72.0 mm at the maximum test load of 8004 kN was also smaller than 100 mm (equal to 10% of the pile diameter). The residual settlement S = 1.5 mm after the full unloading from the working load was also below the limit value S_{ar} = 10.0 mm. All of these values indicated that the pile did not reach the ultimate bearing state. Hence, the TSP1 has a factor of safety greater than 2 against the working load of 4002 kN.

Similar to the case of the TSC1, the calculated distributions of the pile axial forces at different pile head forces ranging from 0.25 to 2.00 times of the working load P_a within 13 steps of the loading and unloading processes for the BOR test are shown in Fig. 32. As seen from the figure, the mobilised shaft resistance and tip resistance increase with increase in the applied head force in the first loading process (steps 1 to 4). At the working load, P_a = 4002 kN, the mobilised tip resistance, Q_b, and the total mobilised shaft resistance, Q_s, were 2174 kN and 1928 kN, respectively, corresponding to about 55% and 45% of the applied force. When unloading to zero (step 8), axial forces remain along the embedment pile length. These residual forces increase with depth and reach a maximum value of about 735 kN at the pile tip. When reloading to the working load at step 9, the axial forces along the pile deeper than 20 m are greater than those in step 4 because of the residual forces in the pile generated in the previous unloading steps. At this applied force, the mobilised tip and shaft resistances were 2565 kN and 1437 kN, respectively, corresponding to 65 % and 35 % of the applied force. When further loads are applied on the pile head in the second loading process (steps 10 to 13), the mobilised shaft resistance and tip

resistance continue to increase, indicating that the pile does not reach the ultimate bearing state at the maximum applied force of 8004 kN.

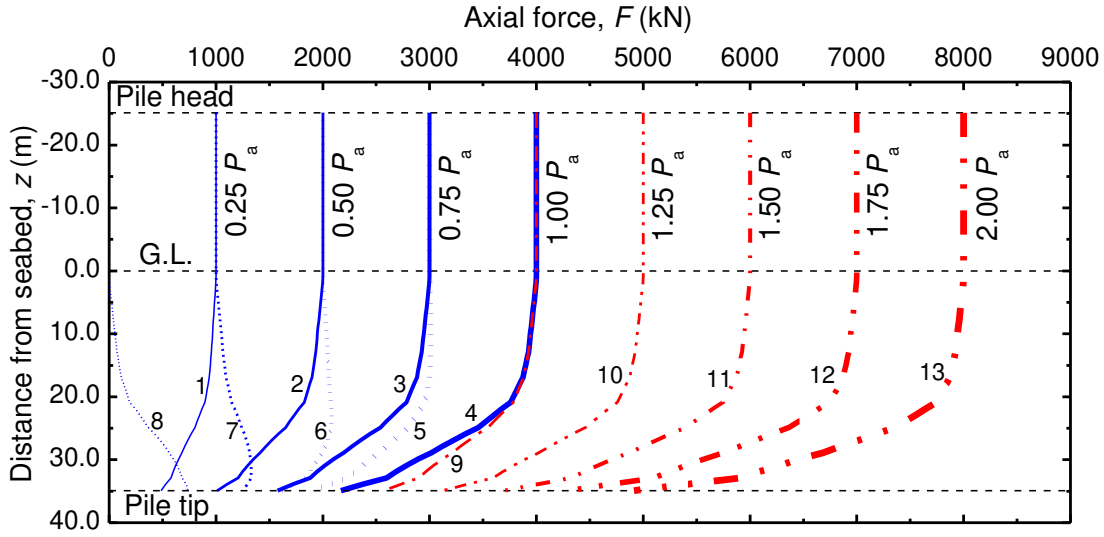

Figure 32. Distribution with depth of pile axial forces at different applied load of TSP1 (D=1000 mm)

As previously mentioned, the TSP1 was actually used as a working pile after the SLT. Hence, in the analysis, the TSP1 was reloaded to the working load after completion of the SLT to predict the pile response when it is used as the working pile. The pile response at the end of the third loading process is indicated by the black dot line in Fig. 33. At the working load of the third loading process, P_a = 4002 kN, the pile axial force reaches a maximum value of 4102 kN at a depth z = 28.9 m (neutral plane) and the mobilised tip and shaft resistance are 3577 kN and 425 kN, respectively. At this applied force, the mobilised tip resistance reaches about 90% of the applied load, which is greater than that in the first loading process at step 4 (55% of P_a) and the second loading process at step 9 (65% of P_a). Because of the higher mobilised tip resistance during this multiple loading process, TSP1 will have smaller safety factor at the pile tip compared to that of the non-tested working piles with the same pile configuration, the same soil and driving conditions.

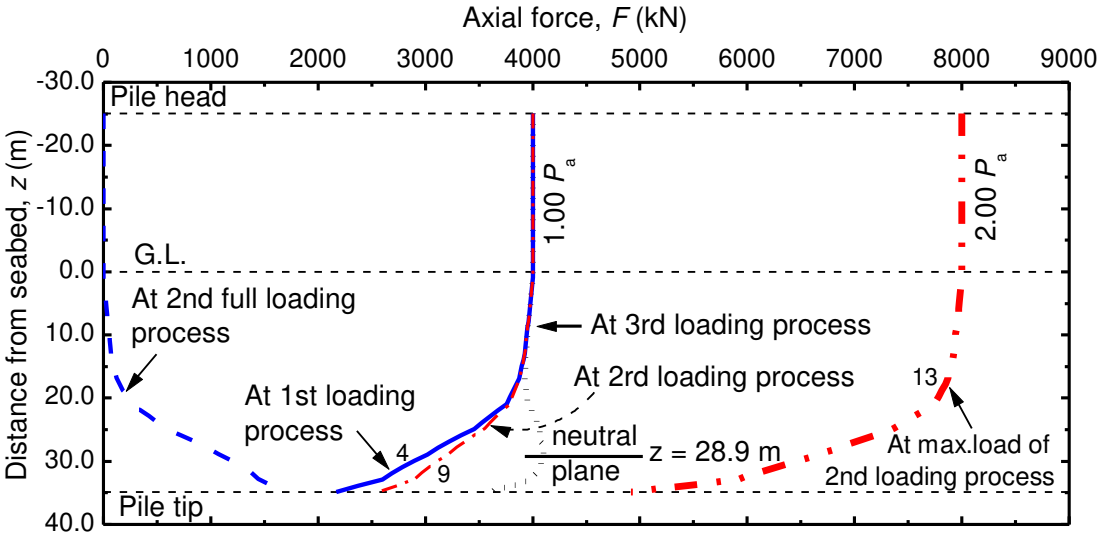

Figure 33. Calculated distributions with depth of the pile axial forces of the TSC1 at BOR test.

In order to estimate the load-displacement behaviour of the TSP1 when it is reused as a working pile after the two loading processes of the SLT, TSP1 was further loaded in the analysis from the working load in the third loading process until the pile reaches the ultimate bearing capacity. The calculated curve is shown in Fig. 34, together with the SLT result. For comparison purposes, the calculated load-displacement curve of the TSP for a monotonic loading is also shown in the figure.

It can be seen from the figure that the yield load and the ultimate bearing capacity of the TSP1 after the two cycles of loading are smaller than those of the TSP1 subjected to only monotonic loading. Here, the yield load is defined as a load corresponding to the maximum curvature on the load-displacement curve, and as defined earlier, the ultimate capacity is a load corresponding to the pile head displacement, S, of 0.1D (S = 100 mm for

the TSP1). It is seen from the comparison of the two calculated relations that loading cycles have a negligible influence on the pile head stiffness of the TSP1, whereas the yield load and the ultimate capacity of the TSP1 subjected to loading cycles are reduced, compared to those of the monotonically loaded TSP1. The values of the ultimate capacity are 8040 kN in the former case and 9640 kN in the latter case, respectively. Reduction of the bearing capacity of the TSP1 due to the double loading process of the SLT is 17 % compared to that of the non-tested pile. In other words, although the non-tested piles would have a safety factor of 2.4, the TSP1 after the SLT would have a safety factor of 2.0 against the design working load of P_a = 4002 when reused as a working pile. Such reduction of the safety factor should be carefully considered when reusing the test pile as a working pile.

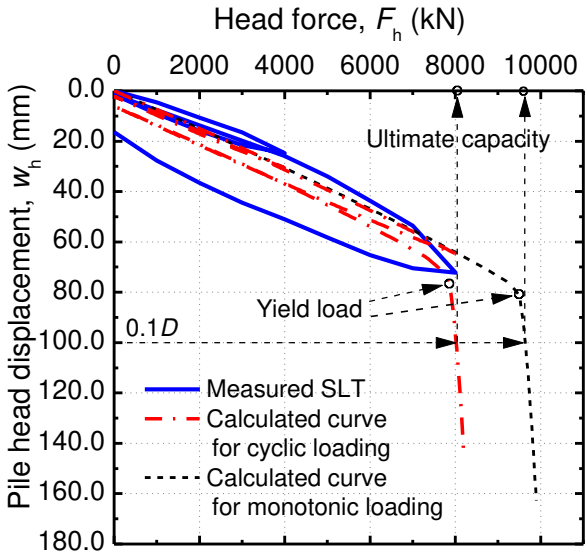

Figure 34. Calculated load-displacement curves with and without cyclic loading, together with the SLT result of TSP1.

Prediction of static load-displacement curves for other test piles

In this part, the static responses of the other two test piles, TSC2 and TSP2, are predicted using the soil parameters identified from the final WMA analyses of TSC1 and TSP1, respectively. The predicted curves are then compared with the load-displacement relations obtained from the static load tests. The specifications of TSC2 and TSP2 have been indicated in Table 2 and the soil profiles have been shown in Fig. 9. The loading and unloading processes were similar to that of the static load test described previously in Fig. 13, with maximum test loads, P_{max}, of 5170 kN for TSC2 and 7716 kN for TSP2, which are two times of the design working load for each pile (see Table 8).

Although the ground at each location of the test piles consisted again of three soil layers of soft clay, clayey sand and hard silt clay, thicknesses of the soil layers vary from location to location as shown in Fig. 9. Hence, for the analyses of the TSC2 and the TSP2, the soil parameters were estimated as follows. In each layer, the average values of the identified soil parameters surrounding TSC1 and TSP1 were used for the soil parameters of TSC2 and TSP2, respectively, while the identified soil parameters at the pile tip and the soil plug base of TSC1 and TSP1 were used for TSC2 and TSP2, respectively.

The predicted and measured curves are shown in Fig. 35 for TSC2 and in Fig. 36 for TSP2. Similarly to TSC1 and TSP1, the ultimate states of these two test piles are not reached at the applied load of $2 \times P_a$ in both the measurements and the calculations. Hence, it can be judged that the TSC2 and TSP2 have a factor of safety greater than 2 against the working loads of 2585 kN and 3858 kN, respectively.

As seen from these two figures, the predicted curves are comparable with the measured ones, indicating that the identified soil parameters of the two tested piles, TSC1 and TSP1, are reasonable. The soil parameters identified from the WMA could be used to adequately estimate the static responses of the other non-tested working piles in this construction site. This means that the WMA of DLTs using the proposed approach can be a practical alternative to the conventional static load test.

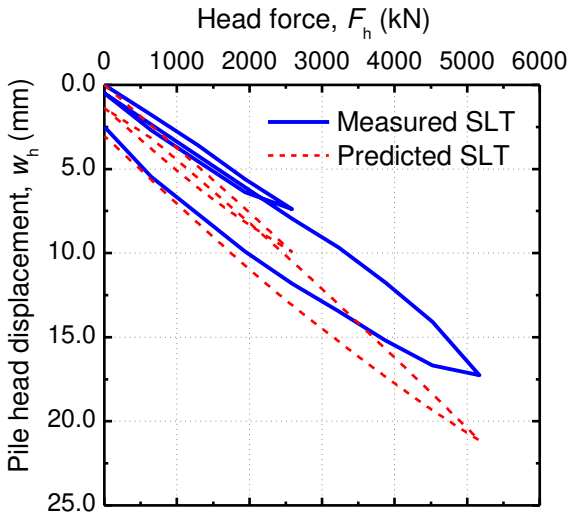

Figure 35. Comparison of the static load displacement curves of the TSC2 (D=800 mm)

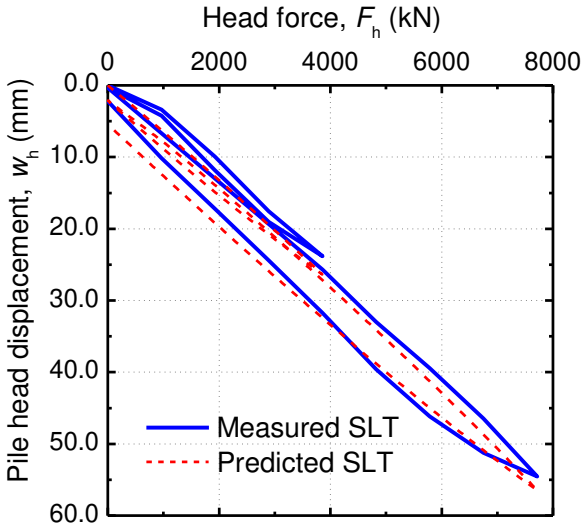

Figure 36. Comparison of the static load displacement curves of the TSP2 (D=900 mm)

CONCLUSIONS

Dynamic and static load tests were conducted on the four test piles with different specifications at the construction site of Thi Vai International Port in Vung Tau province, Viet Nam with the purpose of obtaining the design parameters, selecting the appropriate driving hammer and seeking quality assessment methods for the constructed piles.

This paper first described the test piling in detail including objectives, site conditions, preliminary pile design and results of the SLTs. Then, wave matching analyses (WMAs) of the DLTs of the two test piles, TSC1 and TSP1, at initial driving and re-striking were conducted using the numerical approach developed by the authors, to identify the soil resistance distributions and derive the corresponding static load-displacement relations using the soil parameters identified in the final WMA. Furthermore, the influence of cyclic loading process on the pile response was analytically examined.

The soil parameters identified from the WMAs of the BOR tests were also used to predict the load-displacement relations of the other test piles, TSC2 and TSP2, having different pile configurations and soil profiles from those of TSC1 and TSP1.

The major results of the SLTs and the driving work of the TSC1 and TSP1 are as follows:

1. The bearing capacities of the two test piles exceed two times the design working loads.

2. Termination criteria based on the maximum value of settlement per blow estimated from the Hiley type formula with an ultimate bearing capacity estimated from an empirical equation based on SPT *N*-values can be adequately used for controlling the driving work.

From the WMAs of the TSC1 and TSP1, the following findings and implications were drawn:

3. The static load-displacement curves derived from the final WMAs of DLTs were comparable with the results obtained from the SLTs.
4. The piles which have been subjected to cyclic loading have smaller yield and ultimate capacities compared to the piles subjected to monotonic loading.
5. WMA using the proposed numerical approach can be used to predict the static load-displacement curves of the non-tested working piles based on the identified soil parameters of the tested piles.
6. The "set-up" phenomenon was clearly found from the EOD test, through the BOR test, to the SLT. The thickness of the pile wall might have a great influence on the degree of "set-up" phenomenon.
7. Shear moduli of soils to be used in WMA of piles at this particular site can be estimated from shear moduli at small strain level with reduction factors, about 0.1 for soft soils, 0.15 to 0.20 for medium soils and 0.25 to 0.40 for hard soils.
8. Selection of the pile driving hammer based on the empirical equation in this study is reasonable, because the maximum compressive and tensile stresses along the pile calculated in the WMAs do not exceed the allowable values.

From the SLT results, TSC2 and TSP2 also had the bearing capacities of more than two times the design working loads. Load-displacement curves of TSC2 and TSP2 predicted using the soil parameters identified from the WMAs of TSC1 and TSP1 were comparable with the measured ones. This encourages the use of the WMA procedure proposed by the authors as a practical alternative to the conventional static load test.

Although the applicability of the WMA to quality assessment of constructed piles was demonstrated in this study, it is desired to collect more case histories in Viet Nam for improving the current pile design and pile driving control methods.

ACKNOWLEDGEMENTS

The authors would like to express our appreciation to the VIBROBIS- South VietNam Bridge Road Building Technology Institute, Viet Nam, the ANH VU Geotechnical and Civil Engineering Company, and the Penta-Rinkal Joint Venture for permission of using the static and dynamic load test results in this paper. The authors are thankful to Associate Professor Shun-ichi Kobayashi of Kanazawa University for his encouragements during preparation of this paper.

REFERENCES

Imai, T. (1977). "P- and S-wave velocities of the ground in Japan". Proc. 9th ICSMFE, Tokyo, 2, 257-260. ICSMFE Publisher.

Newmark, NM. (1959). "A method of computation for structural dynamics". Journal of Engineering Mechanics, ASCE 85(EM3), 67-94, American Society of Civil Engineers, Reston VA.

Paikowsky, SG., Whitman, RV. and Baligh, MM. (1989). "A new look at the phenomenon of offshore pile plugging". Marine Geo-resources Geotech., 8, 213-230. Taylor & Francis, Abingdon OX.

Paik, K., Salgado, R., Lee, J. and Kim, B. (2003). "Behaviour of open- and closed-ended piles driven into sand". Journal of Geotechnical and Geo-environmental Engineering, ASCE, 129(4), 296-306, American Society of Civil Engineers, Reston VA.

Phan, T.L., Matsumoto, T. and Kobayashi, S. (2012). "A matrix method of wave propagation analysis in an open-ended pipe pile based on equation of motion". Proc. 9th Int. Conf. on Testing and Design Methods for Deep Foundations, Kanazawa, Japan, 105-112. Kanazawa e-Publishing Co., Ltd.

Randolph, MF., Deeks, AJ. (1992). "Dynamic and static soil models for axial response". Proc. 4th Int. Conf. Application of Stress Wave Theory to Piles, The Hague, 3-14. A.A. Balkema Publishers, Brookfield VT.

ASTM D1143-81. "Standard test method for piles under axial compressive load".

ASTM D4945-00. "Standard test method for high-strain dynamic testing of piles".

TCXDVN 205-1998. "Pile foundation- Specifications for design".

TCXDVN 286-2003. "Pile driving and static jacking works - Standard for construction, check and acceptance".

TCXDVN 269-2002. "Piles- Standard test method for piles under axial compressive load".

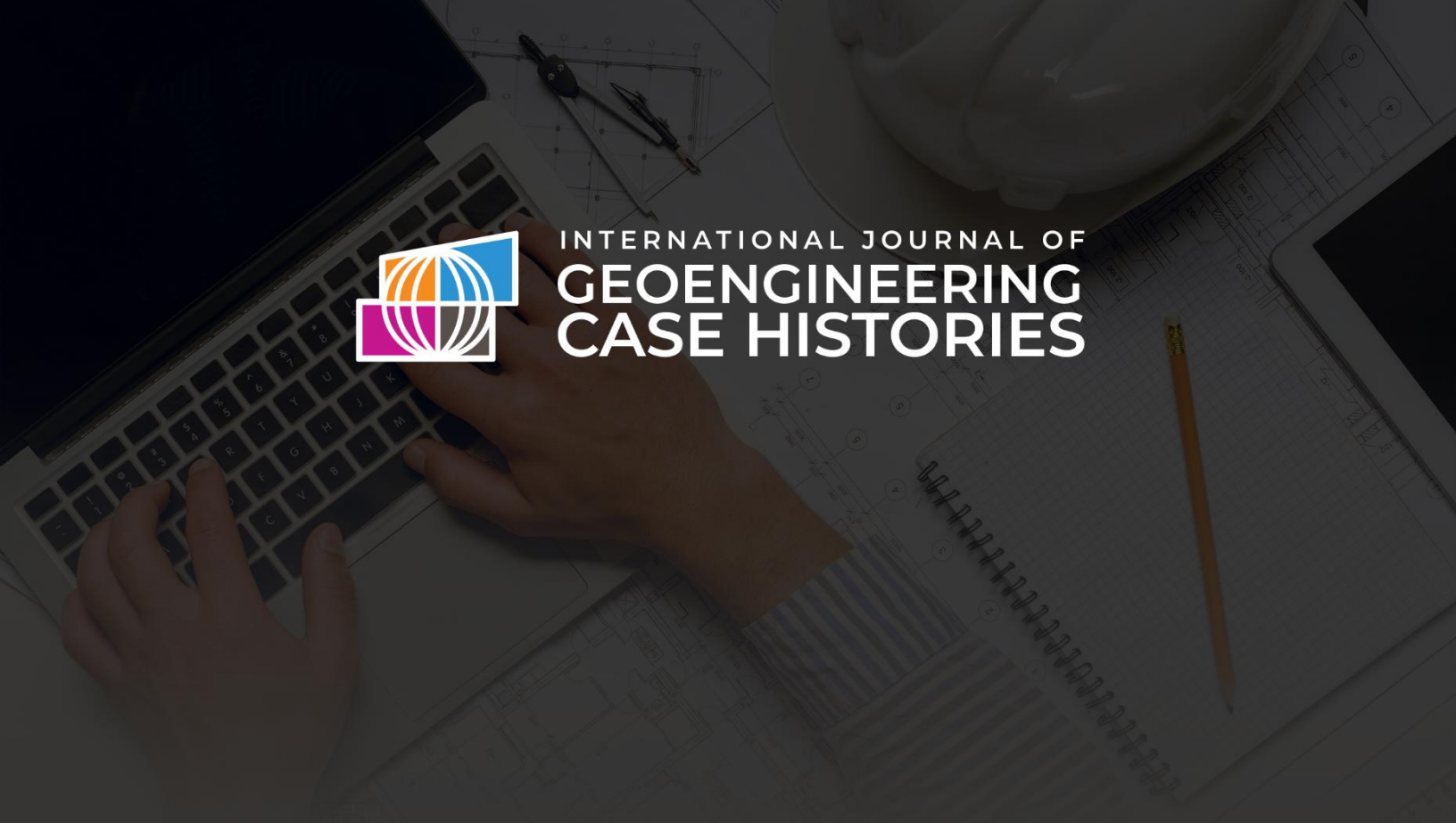

INTERNATIONAL JOURNAL OF
GEOENGINEERING
CASE HISTORIES

The Journal's Open Access Mission is generously supported by the following Organizations: